Mass tracking for chemical analysis: the causes of ozone formation in southern Ontario during BAQS-Met 2007

P.A. Makar[a,*], J. Zhang[a], W. Gong[a], C. Stroud[a], D. Sills[b], K.L. Hayden[a], J. Brook[a], I. Levy[a],C. Mihele[a], M.D. Moran[a], D.W. Tarasick[a], H. He[a]

For submission to ACPD/ACP, revised September 10, 2010

[a] Air Quality Research Division, Science and Technology Branch, Environment Canada, 4905 Dufferin Street, Toronto, Ontario, Canada

[b] National Laboratory for Nowcasting and Remote Sensing Meteorology, Environment Canada, 4905 Dufferin Street, Toronto, Ontario, Canada

*Corresponding Author

Abstract

A three-level nested regional air pollution model has been used to study the processes leading to high ozone concentrations in the southern Great Lakes region of North America. The highest resolution simulations show that complex interactions between the lake breeze circulation and the synoptic flow lead to significant enhancements in the photochemical production and transport of ozone at the local scale. Mass tracking of individual model processes show that Lakes Erie and St. Clair frequently act as photochemical production regions, with average mid-day production rates of up to 4 ppbv per hour. Enhanced ozone levels are evident over these two lakes in 23-day-average surface ozone fields. Analysis of other model fields and aircraft measurements suggests that vertical recirculation enhances ozone levels at altitudes up to 1500m over Lake St. Clair, while strong subsidence enhances ozone over Lake Erie in a shallow layer only 250m deep. The mass tracking of model transport shows that lake-breeze surface

convergence zones combined with the synoptic flow can carry ozone and its precursors hundreds of kilometers from these source areas, in narrow, elongated features. Comparison with surface mesonet ozone observations confirm the presence, magnitude, and timing of these features, which create local ozone enhancements on the order of 20 ppbv above the regional ozone levels.

1 Introduction

The local and mesoscale circulations that arise from contrasts in the heat capacity of land versus water can have a significant effect on air pollution. For large bodies of water (oceans, large lakes), a diurnally varying circulation frequently develops during the warm season. Air over the land is warmed after sunrise while the air over the water is warmed much less, resulting in local pressure differences. These pressure differences drive a local circulation, with air descending over the water and rising over the land during the day, with the reverse occurring at night. This in turn induces daytime divergence at the surface over the water, surface convergence over the land, with a return circulation aloft. The daytime surface divergence and associated water-to-land wind flow is known as the lake- or sea-breeze, while the reverse circulation is referred to as the land breeze (cf. Stull, 1988). The leading edge of the intrusion of marine air onto land may sometimes create a sharp gradient in temperature, wind speed, relative humidity and atmospheric stability; a lake (or sea) breeze front. Air-lake temperature contrasts less than 12C are sufficient to induce this circulation (Laird *et al*., 2001). In light winds, temperature constrasts of only a few degrees are sufficient to induce the circulation – as synoptic wind speeds increase, larger contrasts are required.

Non-reactive tracer modelling studies of coastal Los Angeles noted the ability of sea-breeze-induced fronts (sometimes coupled with topographic effects) to provide sufficient vertical transport to loft pollutants to high levels during the day, in turn creating layers of high concentration pollutants with the onset of more stable conditions at night (Lu and Turco, 1995). This finding has also been found in numerous measurement studies in coastal environments (c.f.

Li, 2004). The sea or lake breeze is often weak with respect to the synoptic flow, but combinations of the two have frequently been shown to give rise to elevated pollution levels. Example locations include Taiwan in the autumn (Cheng, 2002), Houston (Banta *et al*, 2005), Vancouver (Li, 2004), Marseille (Mestayer *et al*, 2005; Lasry *et al*, 2005) , Madrid and Valencia (Millán *et al*., 1997 ; Millán *et al.*, 2000).

Houston is sometimes severely affected by sea-breeze-enhanced ozone levels. Analyses of surface winds, upper level synoptic maps and meteorological conditions have showed that the highest ozone days in that city are associated with the passage of sea-breeze fronts (Darby, 2005; Rappenglück *et al*., 2008). Cluster analysis of surface winds showed that these events correspond to the situation wherein transition from offshore to onshore flow is separated by a period of stagnation greater than or equal to one hour, up to six hours before the ozone event (Darby, 2005). The timing of the arrival of the sea-breeze front is the key factor in predicting high pollution events in Houston, and sea-breezes in opposition to the synoptic flow lead to the highest pollution, due to recirculation of processed air (Banta *et al*., 2005). The depth of penetration of sea-breeze fronts onto land is dependant on the direction of the synoptic wind, as well as on the local radiative balance and land surface characteristics; (Cheng and Byun, 2008), and these factors in turn have a more significant effect on ozone forecasts than, for example, the choice of plume rise parameterization in an air-quality model (Cheng *et al*., 2008). The placement of major emissions sources relative to regularly repeating sea-breeze locations also has a significant impact on both ozone formation and dilution in the Greater Houston area (Byun *et al*., 2007).

The city of Marseille has been another focus for sea-breeze induced meteorological and air pollution studies. High resolution modelling studies have suggested that sea- and lake-breezes interact with Marseille's VOC emissions to create high ozone episodes (Lasry *et al*., 2005). Sophisticated urban heat island modelling for the same region suggests that Marseille's urban heat island circulation is affected by the sea-breeze: the urban circulation when the city was affected by sea-breezes was suppressed relative to instances of synoptic flows originating over

the land (Lemonsu *et al*., 2006a; Drobinski *et al*., 2007). Work by the same group (Lemonsu *et al*., 2006b) suggested the presence of "deep" and "shallow" sea-breeze circulations, the former inhibited by topography, the latter enhanced by topography. Relatively low NO_2 and high O_3 in the Marseille marine boundary layer (indicative of a more photochemically aged airmass) suggest that it is an efficient photochemical reactor (Puygrenier *et al*, 2005). Pollutant concentrations in Marseille maximize just upwind of the sea-breeze front (the front propagation speed is lower than the wind speed, and the vertical mass flux at the front is less than the horizontal flux within the sea-breeze, allowing pollutants to accumulate just behind the front, with some upward transport; (Drobinski *et al*., 2007). The accurate simulation of the fine-scale features of sea-breeze mesoscale transport in the Marseille area is crucial in order to predict both ozone peaks and ozone plumes (Pirovano *et al*., 2007).

The surface temperature during the passage of Marseille's sea-breeze front has been found to be oscillatory (Puygrenier *et al*, 2005; Drobinski *et al*, 2007). Cold air transported inland due to sea-breezes results in temporarily increased stability over the land (isentrope inclination allows the sea-breeze flow to run along the slope, and adiabatic cooling associated with rising air retards the flow). The stability is short-lived, as solar energy is transferred to the surface, triggering turbulent vertical transport including convection. The upward motion results in surface level convergence over the land – this in turn amplifies the sea-breeze flow, which in turn advects cooler air over the land, increasing stability again, and slowing forward motion until the cycle repeats. Recent attempts to model this observed oscillatory flow have been unsuccessful (Drobinski *et al*., 2007).

The two main mechanisms for venting of Marseille's boundary layer air to the free troposphere are upslope winds enhanced by sea breezes, and frontogenesis at the sea-breeze front, with associated turbulence and upward motion (Bastin and Drobinksi, 2006). This venting is of sufficient magnitude to prevent significant recirculation of aged air back into the PBL (Drobinski *et al*., 2007).

Recirculation of aged polluted air in sea-breeze fronts has been observed elsewhere, however. Along the New England coastline, recirculation of aged air in sea-breeze fronts has been observed to increase ozone concentrations by 10 to 30 ppbv (Darby *et al*., 2007). The same study showed the presence of ozone aloft available for downward transport in frontal circulation along with recirculation patterns along the coast, but the observational evidence was not always sufficient to determine the cause of high ozone events (e.g. three possible sources for an event on August 4th, 2004). Recirculation also has a significant impact on pollutants along the eastern Mediterranean (Levy *et al*, 2008). As in the Marseille studies, the interaction between synoptic and mesoscale flow was found to govern the impact of the sea breeze on air pollution. The location of urban heat islands and the shape of the coastline modified the sea-breeze, with the former reducing sea-breeze intensity, and the latter creating convergence regions which intensified it. The mechanism for sea-breeze impacts on eastern Mediterranean ozone levels is unclear, with high ozone levels occurring for both high and low recirculation, and an anti-correlation with NO_x, suggesting both local and long-range transport sources of ozone.

Observational studies of lake-breeze fronts and their impacts on air pollution in the region of the Great Lakes of North America began in the 1960's (Mukammal, 1965; Lyons and Cole 1973, 1976; Lyons and Olsson, 1973; Anlauf et al., 1975). Model simulations of the air pollution associated with lake breeze circulation started with simple Gaussian dispersion models of non-reactive tracers, but the limitations of these models (Lyons *et al*., 1983) led to the use of full mesoscale models at resolutions of 1 to 10 km as the drivers for non-reactive tracer dispersion studies (Lyons *et al*., 1995). The lake-breeze circulation was found to be considerably more complex than previously expected; simulated non-reactive tracer plumes released at the shoreline were entirely transported out of the shallow lake-breeze inflow layer upon reaching the lake-breeze front. Plumes followed helical and even bifurcating trajectories (Lyons *et al*., 1995).

The reactive ozone chemistry associated with lake-breeze fronts in southern Ontario was first examined in the 1980's and 1990's. Some of this early work (e.g., Yap *et al*, 1988)

suggested that local impacts on ozone levels were generally small, while some noted a more significant impact (Mukammal *et al*., 1982, 1985). Ozone concentration increases of 30 ppbv over the course of a few minutes were linked through surface station and satellite observations to the passage of a lake-breeze front in a later, more detailed analysis (Hastie *et al*., 1999). Time-coincident aircraft measurements of precursor NO_x and VOCs suggested that the airmass associated with the ozone maxima was well-aged, and moved inland from a position originating over Lake Ontario.

A common factor of the work to date on lake- or sea-breeze fronts is their complex nature; they are very local-scale features which nevertheless may have a profound impact on surface ozone concentrations in polluted regions. Three-dimensional mesoscale meteorological and air-quality models have provided a useful means of analyzing that complexity in Los Angeles, Houston, Taiwan and Marseille. In the study which follows, we use nested meteorological and pollution models to analyze ozone formation in lake-breeze fronts in southern Ontario. As part of that analysis, we use the concept of mass- or operator-tracking, in which the changes to a pollutant's concentration (in this case, ozone) are tracked through every operator of the air-quality model, allowing us to quantitatively state the relative importance of different processes towards ozone formation in the study region.

The Border Air-Quality Study and Meteorology Study (BAQS-Met) was conducted in the region between Lakes Huron, St. Clair, and Erie, with the aim of studying the impact of lake breezes on local air-quality and long-range-transported chemistry. The study comprised a measurement-intensive field campaign from June 20th to July 10th, 2007, as well as a local monitoring network that operated from the months of June through August. A variety of measurements for particulate matter and gases were carried out at three supersites (Bear Creek, Harrow and Ridgetown), on board the National Research Council of Canada (NRC) Twin Otter aircraft, and on Environment Canada's CRUISER mobile laboratory as part of the study. A ten-

site mesonet monitoring network for 5-minute average ozone and $PM_{2.5}$ was installed in the study region, in addition to ozone and $PM_{2.5}$ observations available from larger scale monitoring networks (AIRNow).

The work that follows has two main components. First, following a discussion on our methodology (section 2), we present a formal statistical evaluation of the model using the available data (section 3). Second, we make use of the model output to infer the physical and chemical causes for ozone formation in the region, using time sequences of model concentration fields, process mass tracking, and comparison of model and observed ozone time series (section 4). The implications of the analysis and concluding remarks are presented in section 5.

2 Methodology

2.1 Modelling System Description

AURAMS (A Unified Regional Air-quality Modelling System) consists of three main components: (a) a prognostic meteorological model, GEM (Global Environmental Multiscale model: Côté *et al*., 1998); (b) an emissions processing system, SMOKE (Sparse Matrix Operator Kernel Emissions: Houyoux *et al*., 2000; CEP, 2003) ; and (c) an off-line regional chemical transport model, the AURAMS Chemical Transport Model (CTM: cf. Cho *et al*., 2009; Gong *et al*., 2006; Makar *et al*.; 2009; Smyth *et al*., 2009; Stroud *et al*., 2008).

GEM version 3.2.2 with physics version 4.5 was run on two domains: a variable-resolution global horizontal grid with a core domain covering North America (575x641 grid points over the globe, with 432x565 grid points over North America, 0.1375° or approximately 15.3-km grid spacing in the core region, 450-s timestep), and a local domain covering the Great Lakes area (565x494 grid points, 0.0225° or approximately 2.5-km grid spacing, 60-s timestep). The model employs 58 hybrid-coordinate levels from the Earth's surface to 10 hPa, with layer thickness increasing monotonically with height. The coarse-grid output was used to provide boundary conditions for the high-resolution domain meteorological simulations (Fig. 1), and the

coarse resolution domain was driven by the operational objective analysis. The standard version of GEM 3.2.2 was modified to include a parameterization for urban heating (Makar *et al*., 2006). Additional improvements included a temperature-gradient-based boundary layer height parameterization, and consistency improvements for the model-generated vertical diffusion coefficients in the lowest model layers.

The GEM meteorology was created in a sequence of 12 hour runs, starting at 0, 6, 12 and 18Z from objective analysis files at those times for the 15-km simulation, the first six hours of these simulations being used for model spin-up, the last six hours being retained for AURAMS simulations. This methodology makes use of the meteorological data assimilation of the objective analysis to the maximum extent, to prevent chaotic drift of the predicted 15-km meteorology from the observations.

Process representations in version 1.4.0 of the AURAMS CTM include emissions from surface and from elevated sources, horizontal and vertical advection, vertical diffusion, gas-phase, aqueous-phase, and inorganic heterogeneous chemistry, secondary organic particle formation, dry and wet deposition, and particle nucleation, condensation, coagulation, sedimentation, and activation. Particulate matter is represented by 12 size bins, each having nine chemical components (Gong *et al*., 2006)

A three level internal nesting setup was used for the AURAMS v1.4.0 simulations: 42-km/15-minute North American domain, in turn driving a 15-km/15-minute Eastern North American domain, in turn driving a 2.5-km/2-minute Southern Ontario domain (Fig. 2). All model resolutions make use of a monthly-varing upper boundary condition for the chemical species, and the outermost domain also makes use of time-invariant and vertically-varying chemical lateral boundary conditions (Makar *et al*., 2010). Twenty-eight terrain-following vertical levels stretched telescopically from the Earth's surface to 18 km, with the first three

levels at 0, 13.9, and 55m AGL. AURMAS' ozone predictions and related diagnostics will be the focus of the current work.

The base year for the anthropogenic emissions processed by SMOKE version 2.2 was 2005 for the U.S.A. and for Canada, and 1999 for Mexico. Biogenic emissions are calculated using BEIS3.09 algorithms, with model generated temperatures and photosynthetically active radiation being used to create these emissions during the model runs.

2.2 Simulation Period and Operating Sequence

Both GEM and the AURAMS CTM were run for the 3-month period from June 1, 2007 to August 31, 2007, for the GEM 15-km domains. The GEM 15-km meteorology was used to drive the AURAMS CTM at both 42 and 15 km for the same time period. The GEM 15-km meteorology was also used for boundary conditions for the higher resolution GEM 2.5-km simulation, in turn used to drive the highest resolution AURAMS 2.5-km simulation. The GEM 2.5-km and AURAMS 2.5-km simulations were only run for dates encompassing the BAQS-Met measurement intensive (June 17 to July 11th, 2007). The lateral boundary conditions for the 15-km and 2.5-km AURAMS CTM simulations were taken from the corresponding coarser resolution simulations in each case; the climatological boundary condition was used for the model top in all three AURAMS simulations.

2.3 Model Diagnostics: Extraction of Model Values and Mass Tracking

2.3.1 Extraction of model values

Times series of surface ozone at hourly intervals were extracted from the 42-km and 15-km AURAMS simulations for comparison to AIRNow observations. Both BAQS-Met mesonet ozone observations (5 minute averages) and AURAMS 2.5-km/2 minute output were summed to create statistically comparable hourly values. Aircraft ozone observations (Hayden *et al*., 2010) were five second resolution data: these were binned to two minutes for comparison to

AURAMS' output time step. The aircraft locations at 10 second intervals during each two minute model step were used to extract the model values along the observed 3D flight path in the model coordinate system, and the average of these values during each 2 minute interval was compared to the observations. The ozone measurements from the mobile laboratory CRUISER were one minute averages: the speed of the mobile laboratory is sufficiently slow that the nearest model gridpoint to the CRUISER location is sufficiently accurate for comparison purposes.

2.3.2 Mass tracking of ozone.

AURAMS v1.4.0 includes an analysis package that records the change in mass of selected model species through each of the model's processes (the components of the net equation are solved as separate operators, Marchuk, 1975), expressed in units of ppbv / hour. These mass tracking options allow comparison of the gas-phase chemical production and loss, the advection, and the diffusion and deposition operators for ozone, within the AURAMS simulations. The relative magnitude and sign of the operators thus give information regarding the reasons for the model's ozone predictions, hence providing hypotheses for ozone formation, destruction, and transport, in the ambient atmosphere. This concept has appeared elsewhere in the literature, as *process analysis* (c.f. Gipson, 1999; Jang et al, 1995; Jeffries and Tonnesen, 1994).

3. Model Performance Evaluation

The model performance for ozone prediction is evaluated here against the available observations, prior to its subsequent use as a tool for analysis of ozone formation in the lower Great Lakes. The performance evaluation thus quantifies the uncertainty associated with the subsequent analysis.

3.1 AURAMS 42-km and 15-km Ozone versus AIRNow Observations.

Summary statistical comparisons between AIRNow and AURAMS hourly ozone at 42-km and 15-km resolutions for the period June 3, 2007 through August 31, 2007 are depicted in Table 1. "42-km East" refers to a subsection of the 42-km domain compatible with the 15-km

domain (left of green line, Fig. 2b), and "15-km BAQS-Met" refers to a subsection of the 15-km domain corresponding to the 2.5-km domain.

The ozone mean biases (MB, Table 1) decrease with increasing resolution, and are positive for all domains and sub-domains. The root mean square error also decreases with increasing resolution. The correlation coefficient *decreases* slightly with increasing resolution. The latter may reflect spatial mis-placement of events becoming more frequent at higher resolution; the low resolution simulations being more likely to capture part of a "near-miss" transport event than high resolution. The mean biases for the different metrics (daily 1 hour maximum, daily mean, and hourly values) are all very similar for the same grids. Overall, the 15-km simulations show a higher statistical "skill" than the 42-km simulations.

3.2 AURAMS 2.5-km Ozone versus Mesonet and Supersite Ozone Observations

Statistical comparisons between the 2.5-km/2-minute AURAMS simulations and the mesonet stations shown in Fig. 3 are given in Table 2. From Table 2, the further increase in model resolution considerably improves the model correlation coefficients relative to the lower resolution simulations of Table 1; mean biases, while now negative, are also of lower magnitude than the lower resolution simulations. Simulated surface ozone therefore has the highest accuracy at the highest model resolution, with the statistics of Table 2 placing limits on the subsequent analysis.

3.3 AURAMS 2.5-km Ozone versus Aircraft Observations.

Statistical comparisons between the 2.5-km/2-minute AURAMS simulations and the entire sequence of flights, and for individual flights, to the aircraft observations, are shown in Table 3. The "All Flights" statistics show a correlation coefficient of 0.74, slope of 0.98, intercept of -7.4 ppbv, a mean bias of -8.4 ppbv, and a mean error of 12.3 ppbv. The correlation coefficients and slopes are improved relative to the monitoring network data in the aforementioned tables, though the biases have become more negative and the mean errors are similar to the monitoring network values. The high resolution model thus has the tendency to be

biased lower for ozone aloft than at the surface. Figure 4 shows the observed time series, simulated time series, correlation scores and mean biases for all flights. Most flights have negative mean biases; the model (thick line on the figures) is biased low relative to the observations (white diamonds).

Both the observations and the model show the presence of relatively short duration changes in the ozone concentration, indicating local-scale perturbations in the ozone field. For example, flight 2 (Fig. 4b) shows peak-to-trough ozone concentration variations of 15 ppbv over durations of 4 minutes, flight 14 (Fig. 4n) shows peak-to-trough variations of 30 ppbv over 26 minute duration in the observations, while the model values show a similar magnitude range but over a shorter duration of about 8 minutes. The typical flying speed of the Twin Otter is 60 m s^{-1}, indicating that these ozone features have trough-to-trough spatial scales of 28 to 94 km. Superimposed on these are even shorter time interval events; for example, Flight 4 (Fig. 4(d)) shows two simulated peaks each of duration 6 minutes (21 km) with peak-to-trough variation of 20 ppbv, while the observed variation in the same part of the time series is about 12 ppbv. Both the observations and the model thus suggest the presence of small spatial-scale ozone features. Our subsequent analysis below (section 4) examines the manner in which these features are formed.

3.4 AURAMS 2.5-km Ozone versus Ozonesonde Observations.

Ozonesonde observations were carried out at the Ridgetown supersite at 12 hour intervals during the study. Model profiles were extracted from each horizontal resolution of the model simulations at the same times as the ozonesonde releases. The 2.5-km model results and the observations are compared in Fig. 5 for the intensive period. Both model and observations show a tropopause fold occurring at the start of the time period (June 20th); ozone concentrations greater than 120 ppbv reach elevations as low as 8 km AGL in the observations. The model shows two later similar events, some indication of which may be present in the observations, but are difficult to distinguish due to missing data. In the model results, these high concentrations

extend down to the 4-km level, while the observations show a shallower penetration, to about the 8-km level. Both observations and simulations show that surface ozone is not significantly enhanced by these fold events, but is rather the result of chemistry and transport close to the ground.

A detailed study of stratospheric/tropospheric exchange during the measurement intensive is presented in He *et al*., (2010). The AURAMS ozone predictions at mid and upper tropospheric levels, and the dependence of these predictions on the manner in which upper and lateral boundary conditions are prescribed have been the focus of a separate research project, reported elsewhere in this issue (Makar *et al*, 2010).

3.5 AURAMS 2.5-km Ozone versus CRUISER Observations

Ozone and other observations were made on the CRUISER mobile laboratory, in transit along roadways in the region, or parked along roadsides, observation sites, or in downtown Windsor. CRUISER driving routes during the intensive are shown in Fig. 6a, and Fig. 6b and 6c compare model and observed O_3 and NO_2, respectively, for the entire period. AURAMS ozone along the CRUISER driving routes is generally biased low (comparing all two minute model values with corresponding averaged observations: mean bias -22 ppbv, mean error 26 ppbv, RMSE 32 ppbv, correlation coefficient (R) 0.56). Nitrogen dioxide was biased high (Fig. 6c), suggesting that the negative biases in the ozone values are the result of excessive NO_x titration of ozone in the model. These biases are much more negative than that seen at the surface mesonet stations (e.g. compare to Table 1, O_3 hourly average mean bias of -3.77 ppbv). The implication is that the model in its current form is unable to capture the very local mixing of freshly emitted NO_x associated with the roadways' mobile sources, but once the NOx has been dispersed to the more rural locations of the mesonet, the fit to the observations improves.

3.6 Summary, Comparisons to Ozone Observations

The above statistical comparisons suggest :

(1) The highest resolution model simulations give the best comparison to observations for surface ozone;

(2) For those simulations, the model has a negative bias at the surface of -2 to -4 ppbv, depending on the metric chosen;

(3) The model compares well to ozonesonde observations over the depth of the troposphere; these suggest that lower tropospheric ozone is not significantly affected by stratospheric intrusions, despite their occurrence during the study period;

(4) The model is biased very low along the roadway networks (-22 ppbv), but this does not affect the regional ozone predictions, suggesting that the low bias is the result of inadequate resolution of the very local scale emissions and turbulence over the roadways;

(5) The surface level negative bias increases to -8.4 ppbv at aircraft altitudes – the aircraft observations and model also suggest the presence of very local-scale features in the ozone concentrations.

4. Model-Predicted Causes of Ozone Formation and Destruction over the Great Lakes

4.1 Case Studies:

We turn now to the use of the model as an analysis tool to explain surface and lower troposphere ozone formation in the study region. During the three-week duration of the measurement intensive, specific patterns of circulation and ozone concentrations tended to recur, depending on the synoptic winds. Three specific patterns occurred with sufficient frequency to be useful as archetypes for the given circumstances for ozone formation. We examine these archetypes below with three case studies (additional case studies are examined in Levy *et al.*, 2010), and then use 23-day averages of model output to explain the underlying causes of enhanced ozone formation in this region.

4.1.1 June 26, July 10 2007: Lake St. Clair lake-breeze front enhancement of ozone north of Detroit

The following example demonstrates the very local nature of ozone enhancements associated with lake-breeze front convergence, how this circulation concentrates precursors, and how it results in downwind ozone increases, even after photochemical production has ceased. Mesoanalysis wind fields and lake-breeze front lines (the latter inferred from the measured winds as well as satellite cloud analysis and radar fine-line analysis, see Sills *et al*, 2010, under review) are shown in Fig. 7a . South of Lake Erie, the lake-breeze front extends up to 50 km inland by 23 UTC (7 pm local daylight time). The lake-breeze front west of Lake Erie and the front from Lake St. Clair create a region of weak surface convergence to the west of Lake St. Clair. The Lake Huron front is pushed northwards over that lake by the synoptic flow. Figure 7b shows the corresponding wind fields and fronts (the latter inferred from convergence regions in the wind fields) predicted by GEM. There is a good correspondence in the locations of the main convergence lines in the vicinity of the lakes between measurements and observations (compare Figs. 7a and 7b), though GEM tended to overpredict convection during this period (gust fronts in Fig. 7b).

Figure 8 shows the corresponding model-predicted surface ozone concentration and wind at 18 and 23 UT (2 pm and 7 pm local time), along a vertical cross-section illustrating the ozone structure through the frontal convergence lines. High concentration (> 100 ppbv) ozone starts to appear by 2pm local time (Fig. 8a,b), and continues to increase through 7 pm local time (8c,d). The location of the ozone maxima is strongly linked to the locations of the lake-breeze front convergence lines; locations “a” and “b” along the cross-section at 18 UT (8b) show that the locations of the high concentrations of ozone extend to 2 km altitude, and correspond to updrafts generated by surface level-convergence.

Figure 9 shows that the ozone is created photochemically in the early afternoon in narrow bands along the convergence zones (e.g. locations “a”, “b”, Fig. 9a), and that this

photochemically produced ozone is transported both upwards and downwind (Fig 9b). By late afternoon, the photochemical production source has shut down leaving only NOx titration removing ozone (blue regions, Fig. 9c), though ozone increases are still occurring due to transport associated with ozone created upwind earlier in the day (red regions, Fig. 9d). These findings are similar to the behind-front net convergence of ozone and precursors noted by Drobinski et al, 2007, with the added information that the regions have a substantial vertical extent.

Observed surface ozone on June 26th is compared to model predictions in Fig. 10, for sites arranged from south to north near the border (Sombra station, Fig. 3, was not operating that day). Model and observations are within 15 ppbv at Paquette Corners (10a) and Bear Creek (10b), while the model is biased -46 ppbv during the ozone maximum at Grand Bend (10c). This large negative bias is apparently due to a small error in the wind direction. Figure 10 (d, e) shows the model-predicted surface ozone concentrations in the area at 18UT and 23UT, respectively, along with the three site locations. High ozone concentrations downwind of the Sarnia plume are predicted by the model in the *vicinity* of Grand Bend, but these remain off-shore for most of the day, and come on-shore to the north-east of the station, in contrast to the observations. The model results suggest that the high values are associated with the Lambton power plant plume. Very similar patterns of ozone formation under south-westerly synoptic winds were observed on other days, with the highest concentrations in the observations and model records occurring at Grand Bend station.

This analysis has several common features with the other examples of model-predicted lake-breeze front ozone formation which follow in subsequent sections: (a) ozone photochemical production just outside precursor source regions in the early afternoon (in subsequent analysis we show that on average these photochemical production areas maximize over the lakes); (b) lake-breeze fronts result in local convergence of both ozone and precursors at the surface and subsequent lofting of these species in the frontal convergence zone, similar to Drobinski *et al*.

(2007); (c) early evening increases in ozone concentration continue in the convergence zones, despite photochemical production having shut down earlier.

4.1.2 July 8, 2007, July 9, 2007, June 27, 2007: Long-range transport of ozone along lake-breeze frontal convergence zones

The previous example showed that frontal convergence lines may be responsible for local ozone enhancements with length scales on the order of 100km. Here, we show that these features may extend for much larger distances. June 27th, July 8th and July 9th were days with moderate south-westerly synoptic winds coupled with strong lake breezes reaching far inland and downwind of the lakes themselves (Sills *et al*, 2010, under review). July 8th is examined here as an example (note that Flight 15 on July 8th, Table 3, has the highest R value of the flight simulations). Figure 11a shows the mesoanalysis front locations at 17UT (1 pm local time), which compare well with the model-predicted wind fields and surface convergence regions (11b). The northern-most convergence line (circled in blue, Fig. 11b) will be examined in more detail (Figs. 12 and 13) Figure 12a shows a time-series comparison between model predictions and observations of surface ozone at Sombra station. The model is biased low by approximately 20 ppbv at night. The model fit is better during the day, when both model and measurements show short time duration enhancements of ozone on the order of 10 to 20 ppbv at midday. Figure 12b shows that the model-predicted surface ozone field at Sombra is part of an elongated feature of high ozone along the more northern of the two convergence lines, a feature extending over 300 km from Detroit to Toronto.

The panels of Fig. 13 show that ozone is photochemically created (red regions, Fig. 13a) between the surface and heights of 1600m above the surface, near the cities and downwind of the region north-east of Lake St. Clair. The ozone production regions are sometimes detached from the surface, with maxima between 1000 and 1400m. Transport (both horizontal and vertical) is removing ozone away from these photochemical production regions (note correspondence of blue areas, 13b., to red areas, 13a). Transport increases the ozone concentrations at elevations above

1600m, downwind and along the surface convergence line (red areas, 13b). Three dimensional surface plotting of the transport terms (not shown) suggests that they are driven by the local flow rather than the synoptic winds; the highest transport levels are along the convergence line.

An ozone cross-section between Lake Huron and Lake Erie across this feature at the same time (Fig. 14) suggests that high concentration ozone is associated with helical circulation in the vicinity of the lake-breeze convergence lines (Fig. 12b shows that the wind field is largely aligned along the length of the convergence zone, while Fig. 14, looking in the direction of that flow, shows a clockwise circulation at 1000m aloft at the cross-section centre, and plumes of ozone becoming detached from the surface in response to these circulation patterns. This helical transport pattern has been noted in other high resolution model simulations (Lyons *et al*., 1995).

As in section 4.1.1, the above analysis suggests that the surface convergence zones associated with lake breezes will increase photochemical ozone production just downwind of precursor source regions by confining and hence increasing precursor concentrations, similar to the findings of Drobinski *et al*. (2007). Ozone concentrations are also enhanced still further downwind, via transport of ozone and its precursors along the convergence line. Extended features of high concentration ozone may become detached from the surface, and travel considerable distances (hundreds of km) downwind of the source regions. These ozone plumes may eventually fumigate downwards, depending on conditions further downwind (for example, the ozone aloft might be brought to the surface on a subsequent day during boundary layer growth, or the ozone aloft may be caught up in a downwind urban heat island circulation).

These regions of enhanced ozone are relatively small (10's of km across, though up to 330 km long, in the above example), and may be difficult to accurately position with a model, relative to the ambient atmosphere. However, observations from the mesoscale monitoring network often capture very similar features in the ozone time series, with the model demonstrating good agreement. An example of this can be seen in the measurement record for July 9th. Figure 15 shows the observed (green) and simulated (blue) time series at Croton (15a)

and Bear Creek (15b). The "spikes" of 20 to 30 ppbv ozone above the "background" diurnal increase/decrease in these time series are the result of the transport of ozone from Lake St. Clair to these stations: this ozone "plume" impacts Sombra station once, and Bear Creek twice, during the period shown, based on analysis of model surface ozone maps (Fig. 16). Mass tracking of the ozone formation and loss processes (not shown) for these times shows that the ozone is photochemically created on the west side of Lake St. Clair – the high ozone "spikes" of Fig. 15 are the result of the local lake-breeze circulation pattern. These observation time series show that very local events associated with lake circulation are capable of enhancing the ozone concentrations by over 20 ppbv relative to the surrounding regions. The model simulations suggest that these events are closely linked to the local circulation in the vicinity of the Lakes. Lake St. Clair in particular is shown in the above example to be a source region for ozone formation.

4.2 Averages of Model Fields: the Average Impact of Transient Events.

The events described above are transient in that they may last over the course of a few hours on any given day. In order to determine the impact of these transient events over a longer time frame, hourly model output for the ozone concentration, mass tracking fields and winds for the 23 days of the intensive were averaged by UT hour. These averages show:

(1) The lake-breeze circulation has a consistent average diurnal pattern;

(2) This circulation has a significant impact on the *average* ozone in the region;

(3) Lakes St. Clair and Erie are regions of intense photochemical ozone production, though the vertical extent of these regions varies greatly between the two lakes;

(4) Helical (re-) circulation of pollutants over the lakes may intensify ozone production there.

4.2.1 UT hour-average surface horizontal winds

Figure 17 shows the 23 day averages of the surface wind field at 12, 16, 20 and 0 UT (8 am, 12 pm, 4pm, and 8 pm local time). By noon (17b), lake-breeze convergence zones (solid

mauve lines) appear on the south west shore of Lake Huron, the west shore of Lake St. Clair, the west and north shores of Lake Erie, and the north shore of Lake Ontario. Each of these lakes in Fig. 17b also contains a region of surface divergence; the outflow from this divergence region perturbs the synoptic flow (limits of this outflow region are indicated by dashed mauve lines). The convergence zones persist through 4pm (17c), and the outflow regions push considerable distances inland. By 8pm (17d) the impact of the lake breezes becomes harder to discern; the average wind speed is sufficiently small to preclude plotting in several locations, probably indicating significant variability in the duration and direction of the surface divergence over the lakes by this time in the evening. The figure shows that the lake-breeze circulation is a sufficiently robust feature that it affects the hourly average wind fields over the lakes.

4.3.2 UT hour-average ozone concentrations

Time-averaged surface ozone concentrations for the same hours as Fig. 17 are shown in Fig. 18. The most significant high concentration ozone features are over Lake Erie, and over the region shared by Detroit, Windsor, and Lake St. Clair (at 4pm, Fig. 18c). The former shows higher ozone on the US than on the Canadian side of Lake Erie – this is due to differences in the emissions databases for the two countries (in Canada, shipping emissions are spatially allocated only along the main shipping lines, in the US, some shipping emissions are spread out over the south side of Lake Erie). The large differences across the border suggest that accurate spatial allocation of shipping emissions is essential for forecasting ozone production over the Great Lakes, and that those emissions may have a significant effect on local ozone production.

The average Lake St. Clair surface ozone at 4 pm (18c) is clearly enhanced within the region of the lake-breeze convergence line and surface outflow (17c). However, it is difficult to distinguish any effect of the long convergence lines discussed earlier, probably due to their relatively short duration and highly time-varying positions, though some features do suggest their presence in the average. Figure 18b shows enhanced ozone concentrations (> 45 ppbv) along the northern Lake Erie coastline and inland, matching the line of the convergence zone of Fig. 17b.

A similar isolated high ozone feature in Fig. 18b matches the location of the Lake Huron outflow and Lake St. Clair convergence line of Fig. 17b.

In order to examine the average ozone over Lakes St. Clair and Erie in more detail, the 23 day average 16 UT ozone concentrations at the surface over the lake, as well as the corresponding cross-sections of ozone concentration, ozone gas-phase production and loss and ozone transport are shown in Fig. 19 a – d. The size of each lake has a significant effect on the ozone production reaction; over Lake St. Clair (left side of cross-sections, 19b), the region of enhanced average ozone extends to elevations of greater than 1500m, while the enhanced ozone production over Lake Erie rises to no more than 250m above the surface. Figure 19c shows that gas-phase photochemical production of ozone is the source of the high concentrations, but once again, the Lake St. Clair source (left side of the cross-section, 19c) has a much greater vertical extent than that over Lake Erie (right side of the cross-section, 19c). The average local gas-phase production rates are relatively high, up to 4 ppbv/hour. The transport pattern (19d) differs between the two lakes. For Lake Erie, transport removes ozone in a thin layer near the surface, and a narrow region of ozone removal extending up to 1500 m is flanked by regions of positive ozone transport. The region of transport removal for Lake St.Clair is larger in horizontal extent, suggesting that at least some of direction of transport is not in the plane of the cross-section.

Figures 17 to 19 suggest that the local diurnal circulation associated with the two Lakes is sufficiently strong to be present in the 23 day average wind fields (17), that this circulation affects the ozone concentrations (18), that the Lakes are photochemical ozone production regions (19), the Lake St. Clair source being a dome roughly 1500 m in height and ~30 km in diameter, and the Lake Erie source being relatively shallow (250m altitude), but encompassing much of the S.W. side of the Lake. A cross-section of the simulated 3D wind field through the 23 day averages across both lakes is shown in Fig. 20, and shows how differences in the circulation over each lake gives rise to their differences in the vertical distribution of gas-phase ozone production. At 8 am (Fig. 20a), vertical winds are relatively light. By noon (20b), a strong vertical circulation has

developed. Updrafts over the north-west shore of Lake St. Clair, likely partially driven by the Detroit heat island ("A" to "B"), and downdrafts over the lake ("B" to "C"), have formed a helical circulation with the synoptic flow, and may allow a recirculation of pollutants over Lake St. Clair. A smaller helical recirculation pattern occurs aloft over Lake Erie, but the larger size of this lake results in net subsidence near the surface. The wind barbs suggest that some air aloft may also reach Lake St. Clair (though the synoptic wind is roughly perpendicular to this cross-section, so the opportunity for the air over Lake Erie to reach Lake St. Clair may be small). By 4pm (Fig. 20b), the Lake St. Clair vertical circulation has intensified and moved southwards, so that the updraft is now on the western shore of the lake itself. The land between the two lakes has become an intense updraft, due to daytime surface heating. These vertical (re) circulations explain the difference in the elevations of the ozone production regions noted above (Fig. 19), and similar features have been noted in the literature (Levy *et al*., 2008).

5. Conclusions

The simulations and comparisons with observations performed here suggest that ozone formation over the southern Great Lakes is significantly enhanced by local circulation and photochemical processing of precursors. Lakes Erie and St. Clair frequently act as photochemical production regions, with average enhancements up to 4 ppbv per hour by early afternoon. The size of the two lakes plays a crucial role in the manner in which ozone production is enhanced, with Lake St. Clair's small size and proximity to Detroit resulting in a "dome" of ozone production on the west side of the lake being released later in the afternoon, and Lake Erie's larger size resulting in strong subsidence over the water with precursor emissions being trapped there in the stable marine boundary layer. Ozone may be transported out of these source regions and the nearby urban areas in lake-breeze circulation convergence lines. These convergence lines result in elongated features of high concentration ozone, extending up to several hundred kilometres. Surface convergence of the local circulation carries the ozone and its precursors aloft and the synoptic wind thus carries the ozone much further downwind. The convergence lines are

transient features lasting for a few hours on any given day, with their magnitude and direction being controlled by the synoptic scale winds. The photochemical production regions over the lakes are very robust features, sufficient to dominate 23-day averages of model-generated ozone concentrations, as well as its production and losses. The local nature of these features suggests that very local-scale emissions controls may have a significant impact on ozone concentrations in this region.

The results have important implications for ozone forecasting in this region. Current air pollution model forecasts generated by the Canadian and U.S. governments operate on 15- and 12-km resolutions, respectively. These resolutions are insufficient to adequately resolve the lake-breeze circulations – while the high-resolution simulations performed here suggest that these same circulations may be responsible for enhancements of the regional ozone concentrations by ~20 ppbv.

While the above results have been statistically compared to observations, it should be noted that uncertainties still exist in the gas-phase mechanisms used in regional models such as AURAMS. The effect of varying chemical mechanisms on ozone formation has been examined in previous work (Kuhn *et al*., 1998), with a 16% R.M.S. error for ozone associated with the choice of chemical mechanism (under polluted conditions), implying that the ozone analysis performed here should be relatively robust. Recent work with newly available HO_x measurement technology (Chen *et al*, 2010) suggest that currently available gas-phase mechanisms may all underestimate HO_x. The authors in the latter study attribute this bias to measurement errors, the effects of unmeasured species, or mechanism errors, some of which are independent of the mechanism used. They found that the differences between mechanisms decreased as the pollutant levels increased, similar to Kuhn *et al*, (1998). Both of these studies suggest that mechanism differences are unlikely to have a significant impact on the work performed here, but they also suggest that further work is needed to determine the cause of this known HO_x deficiency.

Acknowledgements

The authors would like to acknowledge the financial support of Environment Canada and the Ontario Ministry of the Environment for the BAQS-Met study. We gratefully acknowledge the assistance of the AIRNow program and its participating stakeholders.

References

Anlauf, K.G., Lusis, M.A., Wiebe, H.A., and Stevens, R.D.S., 1975. High ozone concentrations measured in the vicinity of Toronto, Canada, Atmos. Environ., 9, 1137-1139.

Banta, R.M., C.J. Senff, J. Nielsen-Gammon, L.S. Darby, T.B. Ryerson, R.J. Alvarez, S.R. Sandberg, E.J. Williams, and M. Trainer, 2005. A bad air day in Houston. *Bulletin of the American Meteorological Society* 86, (5): 657-669.

Bastin, S., Drobinski, P. 2006. Sea-breeze-induced mass transport over complex terrain in south-eastern France: A case-study. *Quarterly Journal of the Royal Meteorological Society* 132 (615): 405-423.

Byun, D.W., Kim, S.-T., Kim, S.-B. 2007. Evaluation of air quality models for the simulation of a high ozone episode in the Houston metropolitan area. *Atmospheric Environment.* 41 (4), 837-853.

CEP, 2003. Carolina Environmental Program, Sparse Matrix Operator Kernel Emission (SMOKE) modelling system, University of North Carolina, Carolina Environmental Programs, Chapel Hill, NC [see http://www.smoke-model.org/index.cfm].

Chen, S., Ren, X., Mao, J., Chen, Z., Brune, W.H., Lefer, B., Rappengluck, B., Flynn, J., Olson, J., Crawford, J., 2010. A comparison of chemical mechanisms based on TRAMP-2006 field data. *Atmospheric Environment*, 44, 4116-4125.

Cheng, F.-Y., Byun, D.W. 2008. Application of high resolution land use and land cover data for atmospheric modeling in the Houston-Galveston metropolitan area, Part I: Meteorological simulation results. *Atmospheric Environment.* 42 (33), 7795-7811.

Cheng, F.-Y., Kim, S., Byun, D.W. 2008. Application of high resolution land use and land cover data for atmospheric modeling in the Houston-Galveston Metropolitan area: Part II. Air quality simulation results *Atmospheric Environment.* 42 (20), 4853-4869.

Cheng, W.-L. 2002. Ozone distribution in coastal central Taiwan under sea-breeze conditions. *Atmospheric Environment.* 36 (21), 3445-3459.

Cho, S., Makar, P.A., Lee, W.S., Herage, T., Liggio, J., Li, S.M., Wiens, B., Graham, L., 2009. Evaluation of a unified regional air-quality modeling system (AURAMS) using PrAIRie2005 field study data: The effects of emissions data accuracy on particle sulphate predictions. *Atmospheric Environmen*t, 43, 1864-1877.

Côté, J., S. Gravel, A. Méthot, A. Patoine, M. Roch, and A. Staniforth, 1998. The operational CMC-MRB Global Environmental Multiscale (GEM) model. Part 1: Design considerations and formulation. *Mon. Wea. Rev.*, **126**, 1373-1395.

Darby, L.S. 2005. Cluster analysis of surface winds in Houston, Texas, and the impact of wind patterns on ozone. *Journal of Applied Meteorology*. 44 (12). 1788-1806.

Darby, L.S., McKeen, S.A., Senff, C.J., White, A.B., Banta, R.M., Post, M.J., Brewer, W.A., Marchbanks, R., Alvarez II, R.J., Peckham, S.E., Mao, H., Talbot, R. 2007. Ozone differences between near-coastal and offshore sites in New England: Role of meteorology. *Journal of Geophysical Research D: Atmospheres*. 112 (16), art. no. D16S91.

Drobinski, P., Saïd, F., Ancellet, G., Arteta, J., Augustin, P., Bastin, P., Brut, A., Caccia, J.L., Campistron, B., Cautenet, S., Colette, A., Coll, I., Corsmeier, U., Cros, B., Dabas, A., Delbarre, H., Dufour, A., Durand, P., Guénard, V., Hasel, M., Kalthoff, N., Kottmeier, C., Lasry, F., Lemonsu, A., Lohou, F., Masson, V., Menut, L., Moppert, C., Peuch, V.H., Puygrenier, V., Reitebuch, O., Vautard, R. 2007. Regional transport and dilution during high-pollution episodes in southern France: Summary of findings from the Field Experiment to Constraint Models of Atmospheric Pollution and Emissions Transport (ESCOMPTE). *Journal of Geophysical Research D: Atmospheres*. 112 (13), art. no. D13105.

Gipson, G.L., 1999. *Chapter 16, Process Analysis, in* Science Algorithms of the EPA Models-3 Community Multiscale Air Quality (CMAQ) Modeling System, Byun D.W., and Ching, J.K.S., United States Environmental Protection Agency, Office of Research and Development, Washington, D.C., EPA/600/R-99/030, 512 pp.

Gong, W., Dastoor, A.P. , Bouchet, V.S. , Gong, S. , Makar, P.A., Moran, M.D., Pabla, B. , Ménard, S. , Crevier, L-P. , Cousineau, S. , and Venkatesh, S., 2006. Cloud processing of gases and aerosols in a regional air quality model (AURAMS) *Atmos. Res*., **82**, 248-275.

Hastie, D. R., J. Narayan, C. Schiller, H. Niki, P. B. Shepson, D. M. L. Sills, P. A. Taylor, Wm. J. Moroz, J. W. Drummond, N. Reid, R. Taylor, P. B. Roussel and O. T. Melo, 1999: Observational evidence for the impact of lake breeze circulation on ozone concentrations in southern Ontario. *Atmospheric Environment*, **33**, 323-335.

Hayden, K., Sills, D. M. L., Li, S., Brook, J., Anlauf, K. G., O'Brien, J. and Sharma, S., 2010. The impact of lake breezes on trace gases and particles during the Border Air Quality and Meteorology Study (BAQS-Met), *Atmospheric Chemistry and Physics Discussions* (under review).

He, H., Tarasick, D.W., Hocking, W.K., Carey-Smith, T.K., Rochon, Y., Zhang, J., Makar, P.A., Osman, M., Brook, J., Moran, M.D., Jones, D., Mihele, C., Wei, J.C., Osterman, G., Argall, P.S., McConnell, J., Bourqui, M., 2010. Transport analysis of ozone enhancement in southern Ontario during BAQS-Met. *Atmospheric Chemistry and Physics Discussions* (under review).

Houyoux, M.R., Vukovich, J.M., Coats, C.J. Jr., and Wheeler, N.J.M., 2000. Emission inventory development and processing for the Seasonal Model for Regional Air Quality (SMRAQ) project. *J. Geophys. Res*., **105**, 9079-9090.

Jang, J-C.C., Jeffries, H.E., and Tonnesen, S., 1995. Sensitivity of ozone to model grid resolution – II. Detailed process analysis for ozone chemistry. *Atmospheric Environment*, **29**, 3101-3114.

Jeffries, H.E., and Tonnesen, S., 1994. A comparison of two photochemical reaction mechanisms using mass balance and process analysis. *Atmospheric Environment*, **28**, 2991-3003.

Kuhn, M., Builtjes, P.J.H., Poppe, D. Simpson, D., Stockwell , W.R. and Andersson-Skoeld, Y., Baart, A., Das, M., Fiedler, F., Hov, O., Kirchner, F., Makar, P.A., Milford, J.B., Roemer, M.G.M., Ruhnke, R.., Strand, A., Vogel, B., Vogel, H., 1998. Intercomparison of the Gas-Phase Chemistry in Several Chemistry and Transport Models. *Atmospheric Environ*ment **32**, 693-709.

Laird, N.F., Kristovich, D.A.R., Liang, X.-Z., Arritt, R.W., Labas, K. 2001. Lake Michigan lake breezes: climatology, local forcing, and synoptic environment. *Journal of Applied Meteorology*, 40 (3), 409-424.

Lasry, F., Coll, I., Buisson, E. 2005. An insight into the formation of severe ozone episodes: Modeling the 21/03/01 event in the ESCOMPTE region. *Atmospheric Research*, 74 (1-4), 191-215.

Lemonsu, A., Bastin, S., Masson, V., Drobinski, P. 2006a. Vertical structure of the urban boundary layer over Marseille under sea-breeze conditions. *Boundary-Layer Meteorology*, 118 (3), 477-501.

Lemonsu, A., Pigeon, G., Masson, V., Moppert, C. 2006b. Sea-town interactions over Marseille: 3D urban boundary layer and thermodynamic fields near the surface. *Theoretical and Applied Climatology*, 84 (1-3), 171-178.

Levy, I., Makar, P.A., Sills, D., Zhang, J., Hayden, K.L., Mihele, C., Narayan, J., Brook, J., 2010. Unravelling the complex local scale flows influencing ozone patterns in the southern Great Lakes, *Atmospheric Chemistry and Physics Discussions* (under review).

Levy, I., Dayan, U., Mahrer, Y. 2008. A five-year study of coastal recirculation and its effect on air pollutants over the East Mediterranean region. *Journal of Geophysical Research D: Atmospheres*. 113 (16), D16121.

Li, S.M. 2004. A concerted effort to understand the ambient particulate matter in the Lower

Fraser Valley: The Pacific 2001 Air Quality Study. Atmospheric Environment, **38** (34), 5719-5731.

Lu, R. and R.P. Turco, 1995. Air Pollutant Transport in a Coastal Environment - II. Three-Dimensional Simulations over Los Angeles Basin. *Atmos.-Env.* **29**:1499-1518.

Lyons, W. A. and H. S. Cole, 1973. Fumigation and Plume Trapping on the Shores of Lake Michigan During Stable Onshore Flow, *Journal of Applied Meteorology*, **12**, 494–510.

Lyons, W.A. and H.S. Cole, 1976. Photochemical Oxidant Transport: Mesoscale Lake Breeze and Synoptic-Scale Aspects, *Journal of Applied Meteorology*, **15**, 733–743.

Lyons, W.A. and L.E. Olsson, 1973. Detailed Mesometeorological Studies of Air Pollution Dispersion in the Chicago Lake Breeze. *Mon. Wea. Rev.* **101**:387-403.

Lyons, W.A., R.A. Pielke, C.J. Tremback, R.L. Walko, D.A. Moon, C.S. Keen, 1995. Modeling Impacts of Mesoscale Vertical Motions upon Coastal Zone Air Pollution Dispersion. *Atmos.-Env.* **29**:283-301

Lyons W.A., Keen, C.S., and Schuh, J.A., 1983. Modeling mesoseale diffusion and transport processes for releases within coastal zones during land/sea breezes. U.S. Nuclear Regulatory Commission, NUREG/CR-3542, Washington, DC, 202 pp.

Makar, P.A., Gravel, S., Chirkov, V., Strawbridge, K.B., Froude, F., Arnold, J., and Brook, J., 2006: Heat flux, urban properties, and regional weather, Atmos. Environ., 40, 2750-2766.

Makar, P.A., Moran, M.D., Zheng, Q., Cousineau, S., Sassi, M., Duhamel, A., Besner, M., Davignon, D., Crevier, L.-P., and Bouchet, V.S.: Modelling the impacts of ammonia emissions reductions on North American air quality, *Atmos. Chem. Phys.*, **9**, 7183-7212, 2009.

Makar, P.A., Gong, W., Mooney, C., Zhang, J., Davignon, D., Samaali, M., Moran, M.D., He, H., Tarasick, D.W., Sills, D., and Chen, J., 2010. Dynamic ozone boundary conditions for air-quality forecasts, *Atmospheric Chemistry and Physics, accepted, September 2010*.

Marchuk, G.I., 1975. *Methods of numerical mathematics*, Springer-Verlag, New York, 316pp.

Mestayer, P.G., P. Durand, P. Augustin, S. Bastin, J-M. Bonnefond, B. Bénech, B. Campistron, A. Coppalle, H. Delbarre, B. Dousset, P. Drobinski, A. Druilhet, E. Fréjafon, C.S.B. Grimmon, D. Groleau, M. Irvine, C. Kergomard, S. Kermadi, J-P. Lagouarde, A. Lemonsu, F. Lohou, N. Long, V. Masson, C. Moppert, J. Noilhan, B. Offerle, T.R. Oke, G. Pigeon, V. Puygrenier, S. Roberts, J-M. Rosant, F. Saïd, J. Salmond, M. Talbaut, and J. Voogt. 2005. The Urban Boundary-Layer Field Campaign in Marseille (UBL/CLU-ESCOMPTE): Set-Up and First Results. Boundary-Layer Meteorology. 114, 315-365.

Millán, M.M., Salvador, R., Mantilla, E., Kallos, G., 1997. Photooxidant dynamics in the Mediterranean basin in summer: Results from European research projects. Journal of Geophysical Research, 102, 8811-8823.

Millán, M.M., Mantilla, E., Salvador, R., Carratalá, A., Sanz, M.J., Alonso, L., Gangoiti, G., Navazo, M., 2000. Ozone cycles in the western Mediterranean basin: interpretation of monitoring data in complex coastal terrain. J. Applied Met., 39, 487-508.

Mukammal, E.I., 1965. Ozone as a cause of tobacco injury. Agricultural Meteorology, 2, 145-165.

Mukammal, E.I., H.H. Neumann and Gillespie, T.J., 1982. Meteorological Conditions Associated with Ozone in Southwestern Ontario, Canada. *Atmos. Env.* **16**:2095-2106.

Mukammal, E.I., H.H. Neumann and T.R. Nichols, 1985. Some Features of the Ozone Climatology of Ontario, Canada and Possible Contributions of Stratospheric Ozone to Surface Concentrations. *Arch. Met. Geoph. Biocl.* **34**:179.

Pirovano, G., Coll, I., Bedogni, M., Alessandrini, S., Costa, M.P., Gabusi, V., Lasry, F., Menut, L., Vautard, R. 2007. On the influence of meteorological input on photochemical modelling of a severe episode over a coastal area. *Atmospheric Environment*, 41 (30), pp. 6445-6464.

Puygrenier, V., Lohou, F., Campistron, B., Saïd, F., Pigeon, G., Bénech, B., Serça, D. 2005. Investigation on the fine structure of sea-breeze during ESCOMPTE experiment. *Atmospheric Research*, 74 (1-4), 329-353.

Rappenglück, B., Perna, R., Zhong, S., Morris, G.A. 2008. An analysis of the vertical structure of the atmosphere and the upper-level meteorology and their impact on surface ozone levels in Houston, Texas. *Journal of Geophysical Research D: Atmospheres*, 113 (17), D17315.

Sills, D., Brook, J., Taylor, P., Zhang, J., Levy, I., Makar, P.A., Hayden, K., 2010. Lake breezes in the southern Great Lakes and their influence during BAQS-Met2007, *Atmospheric Chemistry and Physics Discussions* (under review).

Smyth, S.C., Jiang, W., Roth, H., Moran, M.D., Makar, P.A., Yang, F., Bouchet, V.S., and Landry, H., 2009: A comparative performance evaluation of the AURAMS and CMAQ air quality modelling systems. Atmos. Environ., 43, 1059-1070.

Stroud, C. A., G. Morneau, P. A. Makar, M. D. Moran, W. Gong, B. Pabla, J. Zhang, et al. 2008. OH-reactivity of volatile organic compounds at urban and rural sites across canada: Evaluation of air quality model predictions using speciated VOC measurements. *Atmospheric Environment* 42, (33), 7746-7756.

Stull, R.B., 1988. *An Introduction to Boundary Layer Meteorology*, Kluwer Academic Publishers, Boston, 666pp.

Yap, D., D.T. Ning and W. Dong, 1988. An assessment of source contributions to the ozone concentrations in southern Ontario. 1979-1985. *Atmos. Env.* **22**:1161-1168.

Tables:

Table 1: Evaluation statistics for 2007/06/03 – 2007/08/31, 42-km and 15-km AURAMS versus AIRNow. M_obs = observed mean, M_mod = model mean, MB = mean bias, NMB = normalized mean bias, R = correlation coefficient, RMSE = root mean square error.

	O_3 daily 1-hour max				**O_3 daily mean**				**Hourly O_3**			
	42-km	15-km	42-km east	15-km "BAQS Met"	42-km	15-km	42-km east	15-km "BAQS-Met"	42-km	15-km	42-km east	15-km "BAQS-Met"
Number of sites	1167	681	833	61	1167	681	833	61	1167	681	833	61
M_obs (ppbv)	56.9	57.7	55.6	57.9	32.6	33.3	31.7	33.6	33.0	33.7	32.1	34.0
M_mod (ppbv)	65.2	63.5	64.0	63.6	43.6	40.0	42.9	40.0	43.8	40.3	43.1	40.2
MB (ppbv)	8.4	5.8	8.4	5.7	11.0	6.7	11.3	6.5	10.8	6.5	11.0	6.2
NMB	0.16	0.10	0.16	0.10	0.38	0.22	0.37	0.21	0.37	0.21	0.36	0.19
R	0.46	0.44	0.49	0.44	0.43	0.39	0.46	0.33	0.60	0.61	0.63	0.61
RMSE (ppbv)	19.3	18.2	18.3	18.1	16.0	13.2	15.3	14.1	20.5	18.5	19.7	18.5

Note: "42-km east" denotes statistics computed for sites east of 100 W within the continental 42-km domain; "BAQS-Met" denotes statistics computed for sites within an area bound by 40.5 – 44.5 N and 84 – 78 W. Number of stations: 42-km: 1167, 42-km east: 833, 15-km: 681, 15-km "BAQS-Met": region bounded by 40.5 to 44.5N and 78 to 84 W.

Table 2: Ozone statistics at all BAQS-Met surface mesonet stations, 2.5-km resolution simulations

Statistic	**O_3 hourly averages**	**O_3 daily mean**	**O_3 daily 1-hour max**	**O_3 daily 1-hour min**
M_obs (ppbv)	41.2	41.8	63.2	21.5
M_mod (ppbv)	37.4	38.1	61.2	18.7
MB	-3.77	-3.78	-1.93	-2.83
NMB	-0.092	-0.090	-0.031	-0.132
R	0.63	0.60	0.57	0.60
RMSE (ppbv)	17.6	13.2	17.9	13.2

Table 3:

Flight Number	R	Slope	Intercept	Mean Bias	Normalized Mean Bias	Mean Error	Normalized Mean Error	Number of Points
All Flights	**7.40E-01**	**9.834E-01**	**-7.42E+00**	**-8.42E+00**	**-1.39E+01**	**1.23E+01**	**2.04E+01**	**939**
1 (06/23 12:54 – 15:00)	6.65E-01	9.82E-01	-1.21E+01	-1.27E+01	-3.94E+01	1.27E+01	3.84E+01	56
2 (06/23 17:22 – 19:56)	2.83E-01	4.17E-01	1.18E+01	-1.15E+01	-2.87E+01	1.15E+01	2.89E+01	70
3 (06/23 21:34 – 22:16)	2.85E-01	2.76E-01	1.42E+01	-1.49E+01	-3.70E+01	1.49E+01	3.70E+01	15
4 (06/25 14:38 – 17:24)	5.39E-01	9.81E-01	-1.08E+01	-1.20E+01	-1.85E+01	1.26E+01	1.95E+01	67
5 (06/25 19:30 - 21:54)	5.27E-01	5.86E-01	1.81E+01	-1.20E+01	-1.65E+01	1.39E+01	1.91E+01	68
6 (06/25 23:00– 06/26 0:00)	-2.03E-02	-2.02E-02	6.21E+01	-1.16E+01	-1.60E+01	1.18E+01	1.63E+01	23
7 (06/26 12:34 – 15:06)	-2.10E-01	-1.78E-01	7.71E+01	-3.12E+00	-4.59E+00	7.55E+00	1.11E+01	67
8 (06/26 17:20 – 19:04)	4.01E-01	2.73E-01	4.87E+01	-3.01E+00	-4.23E+00	5.87E+00	8.25E+00	48
9 (06/26 20:10 – 22:20)	4.10E-01	5.77E-01	2.67E+01	-3.01E+00	-4.28E+00	9.13E+00	1.30E+01	61
10 (06/27 12:30– 13:42)	4.78E-01	1.00E+00	-6.33E-02	-5.27E-02	-1.20E-01	6.38E+00	1.46E+01	28
11 (06/27 15:10– 17:40)	6.22E-01	5.64E-01	3.37E+01	6.45E+00	1.03E+01	9.19E+00	1.47E+01	64
12 (07/03 22:44–07/04 13:00)	3.84E-01	4.32E-01	1.24E+01	-2.50E+01	-3.79E+01	2.50E+01	3.80E+01	71
13 (07/07 8:18 – 11:16)	3.66E-01	2.00E-01	1.85E+01	-1.78E+01	-3.92E+01	1.83E+01	4.02E+01	77
14 (07/07 17:30–20:20)	-4.27E-02	-5.51E-02	4.99E+01	-1.72E+01	-2.70E+01	1.86E+01	2.92E+01	75
15 (07/08 15:20–18:12)	7.33E-01	1.37E+00	-2.07E+01	4.09E+00	6.17E+00	8.59E+00	1.29E+01	76
16 (07/08 22:20– 07/09 1:00)	3.97E-01	7.82E-01	1.48E+01	-4.81E-01	-6.89E-01	6.08E+00	8.70E+00	73

List of Figure Captions

(1) GEM 15-km and 2.5-km domains.

(2) AURAMS 42-km, 15-km and 2.5-km domains.

(3) Locations of BAQS-Met surface mesonet stations

(4) (a-h) Observed and simulated O3 (ppbv), first 8 flights.

(4) (i-p) Observed and simulated O3 (ppbv), remaining 8 flights.

(5) (a) Observed ozone profiles from sondes, (b) Model-simulated ozone profiles.

(6) (a) CRUISER driving routes during the intensive, (b) Observed and model-simulated ozone along CRUISER driving routes, (c) Observed and simulated NO2 along CRUISER driving routes.

(7) June 26th , 23 UT (7pm local time) (a) Meso-analysis lake-breeze front locations; (b) Lake-breeze front locations inferred from convergence pattern of 2.5-km resolution model winds.

(8) Model-predicted fields for June 26th. 18UT (2pm local time): (a) Surface ozone and wind barbs; (b) Vertical profile of ozone and winds along cross-section A-B. (c,d): As in (a,b), but at 23UT (7 pm local time).

(9) 18UT (2pm local time): (a) Gas-phase photochemical production and loss along cross-section A-B of Fig. 8; (b) Total transport rate of change of ozone along cross-section A-B of Fig 8. (c,d): As in (a,b), but at 23UT (7 pm local time).

(10) Ozone comparison with surface observations, June 26th, at (a) Paquette Corners, (b) Bear Creek, (c) Grand Bend. Model surface ozone concentrations at (d) 18UT and (e) 23 UT.

(11) (a) Meso-analysis lake-breeze front locations on July 8th, 17UT (1pm local time); (b) Model-predicted surface wind field and convergence zones.

(12) (a) Model-predicted ozone versus observations, July 8th, Sombra station. (b) Model-predicted surface ozone and surface winds at 17 UT (1 pm local time)

(13) Model-predicted ozone mass tracking fields for July 8th, 17UT (1 pm local time), Detroit to Toronto cross-section. (a) Gas-phase photochemical production, and loss; (b) Total Total transport rate of change

(14) Model-predicted ozone and wind fields, July 8, 17 UT, Lake Huron to Lake Erie cross-section.

(15) Model-predicted surface ozone and wind fields for July 9th at (a) Croton, (b) Bear Creek. Statistical measures are for the entire measurement intensive, at each site.

(16) Model-predicted surface ozone and wind fields for July 9th, (a) 17UT (1 pm local time); (b) 19 UT (3 pm); (c) 20 UT (4pm); (d) 22 UT (6pm). SOM: Sombra station. CRO: Croton station. Lambton P.P. = Lambton Power-Plant.

(17) 23 day average wind fields at (a) 12UT, (b) 16 UT, (c) 20 UT, and (d) 0 UT; 8 am, 12 pm, 4 pm and 8 pm, respectively. Convergence regions marked as solid mauve lines, boundary of divergence outflow regions marked with dashed mauve lines.

(18) 23 day average ozone concentration fields at (a) 12UT, (b) 16 UT, (c) 20 UT, and (d) 0 UT; 8 am, 12 pm, 4 pm and 8 pm, respectively.

(19) 23 day average values at 20Z (4 pm local time): (a) Surface ozone over Lake St. Clair and Lake Erie, showing location of cross-section used for (b) ozone concentration, (c) ozone gas-phase production and loss, (d) ozone total transport..

(20) Cross-section of 3D wind fields across Lakes St. Clair and Erie at (a) 12UT (8am), (b)_ 16UT (12 noon), and (c) 20 UT (4pm). Net upward motion streamlines are sketched in red, downward motion in blue. Inset: location of the cross-section, superimposed on 20UT surface winds.

Figure 1: GEM 15-km and 2.5-km domains

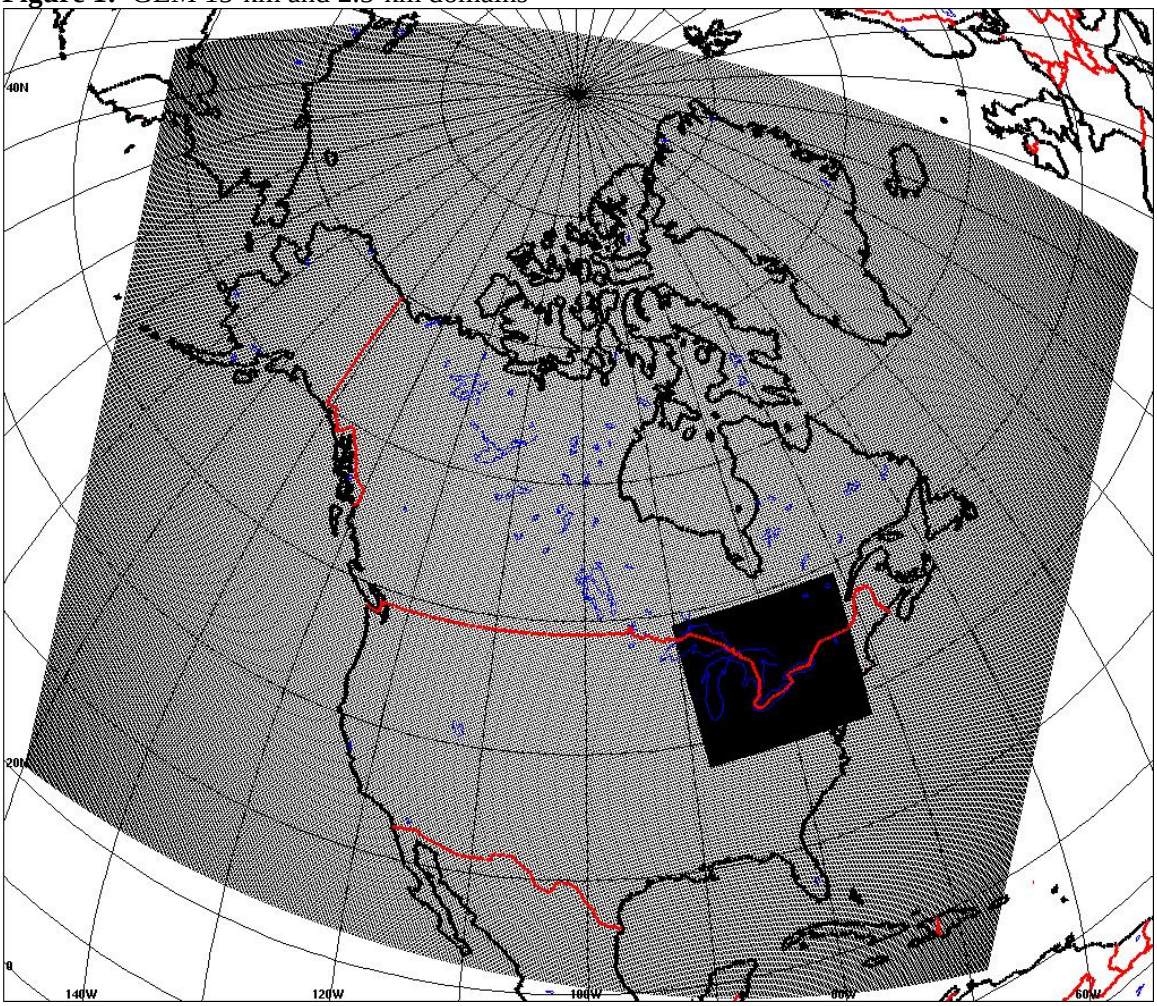

Figure 2: (a) AURAMS 42-km, 15-km, and 2.5-km domains, (b) monitoring stations used for 42km comparison to observations (Mean Bias shown; region east of 100W is "42-km-East"); (c) monitoring sites used for 15-km comparison to observations (Mean Bias shown).

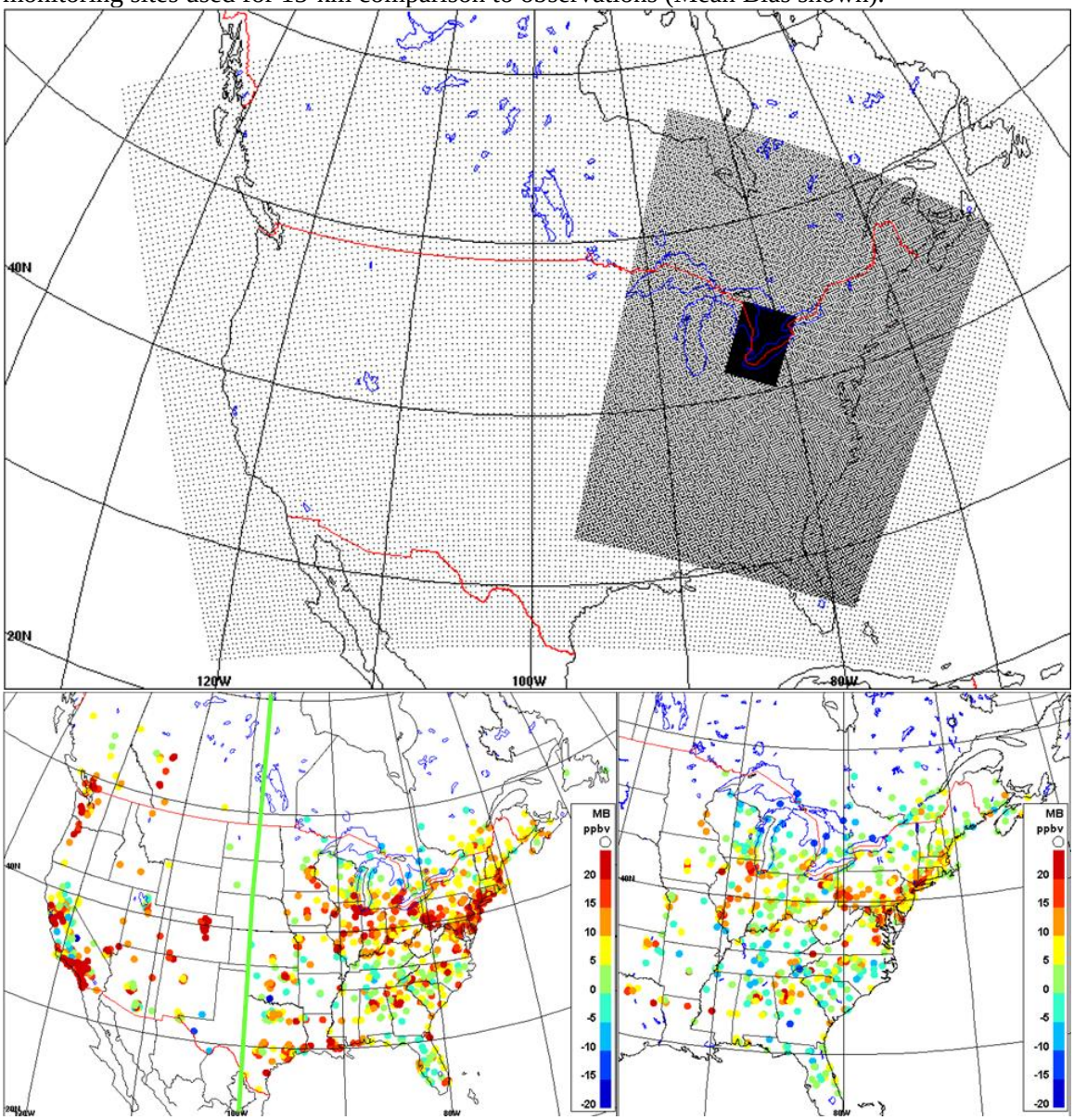

Figure 3: Locations of BAQS-Met surface mesonet stations.

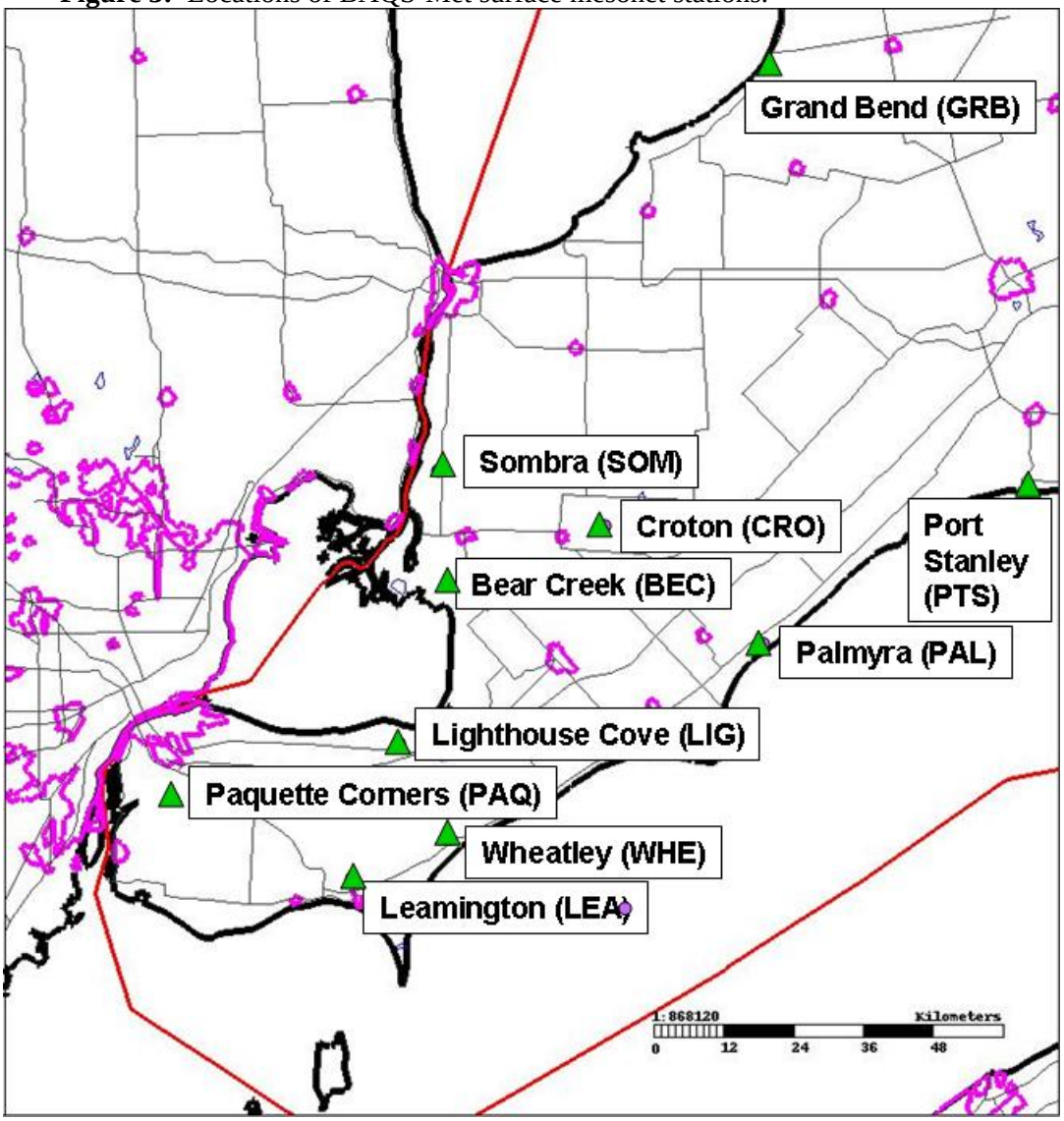

Figure 4 (a-h): Observed and simulated O3 (ppbv), first 8 flights.

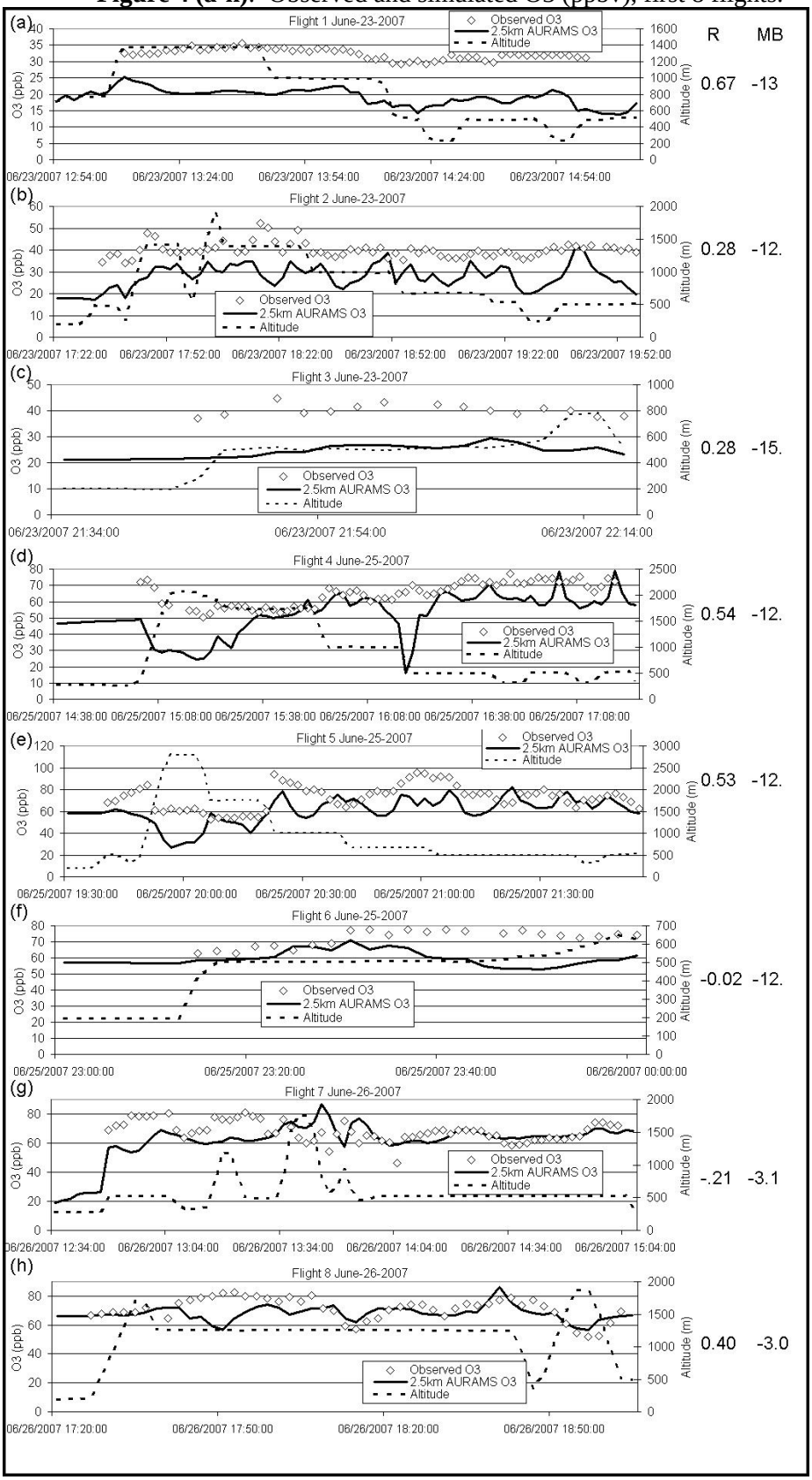

Figure 4 (i-p): Observed and simulated O3 (ppbv), remaining 8 flights.

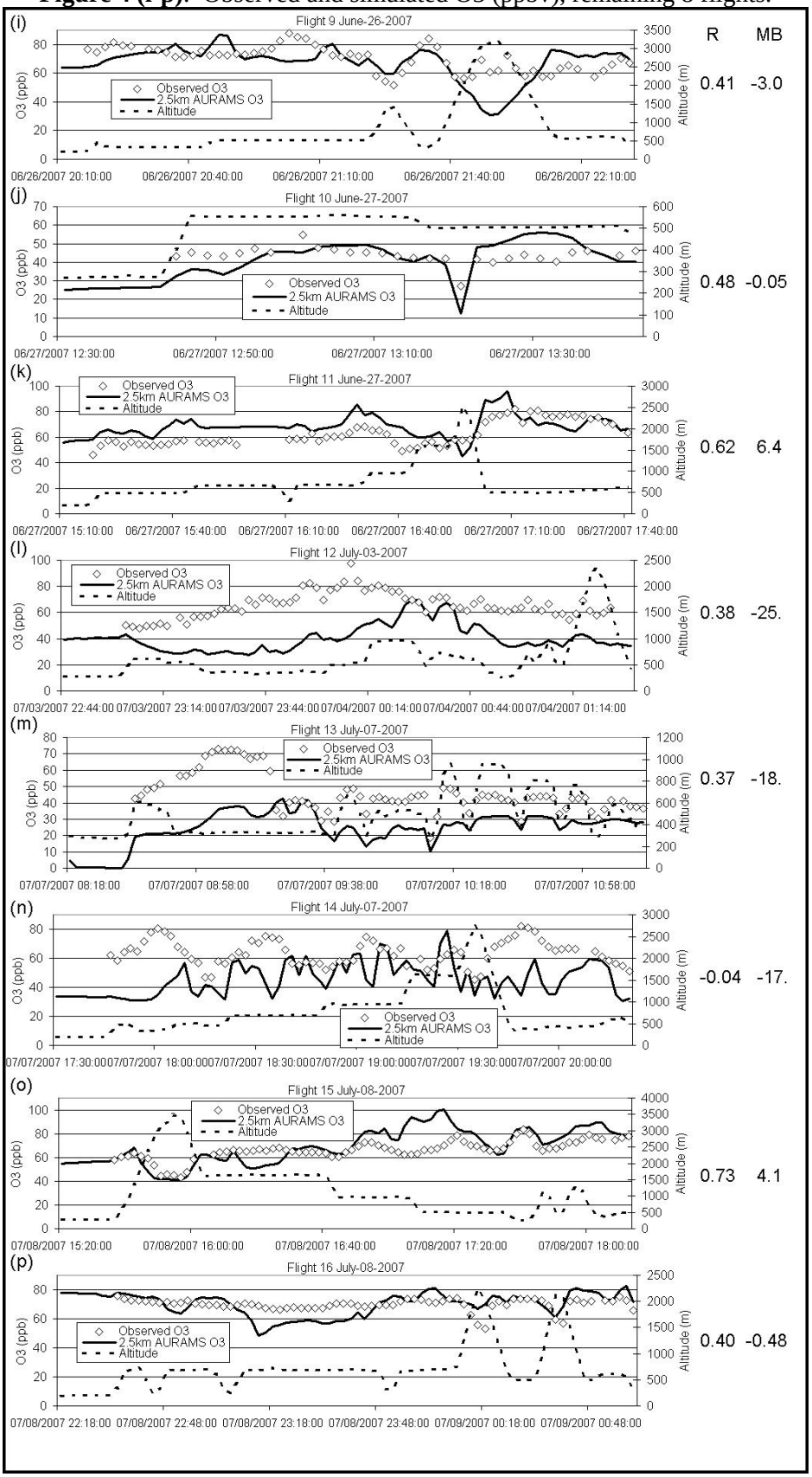

Figure 5: (a) Observed ozone profiles from sondes, (b) Model-simulated ozone profiles.

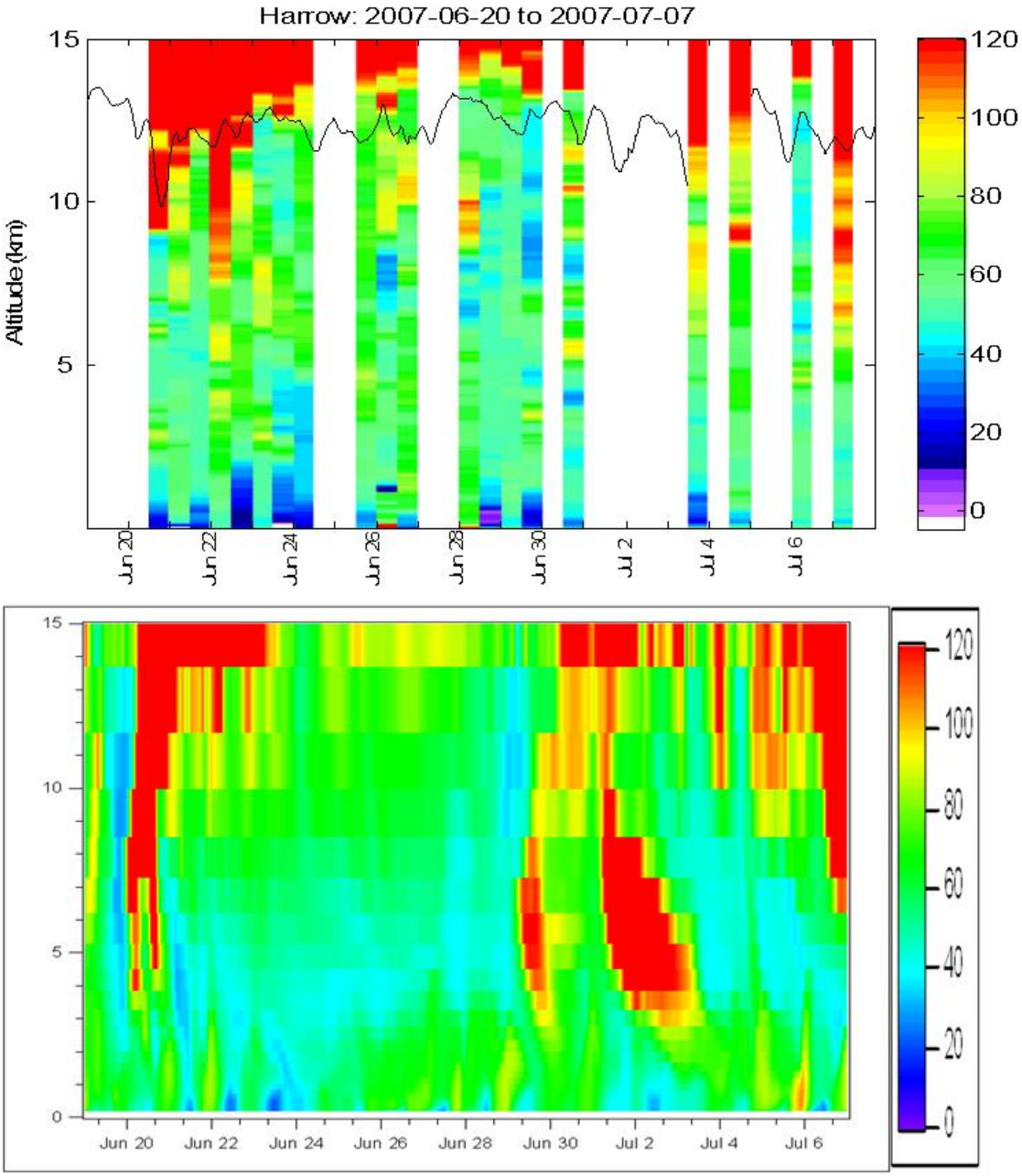

Figure 6: (a) CRUISER driving routes during the intensive, (b) Observed and model-simulated ozone along CRUISER driving routes, (c) Observed and simulated NO2 along CRUISER driving routes.

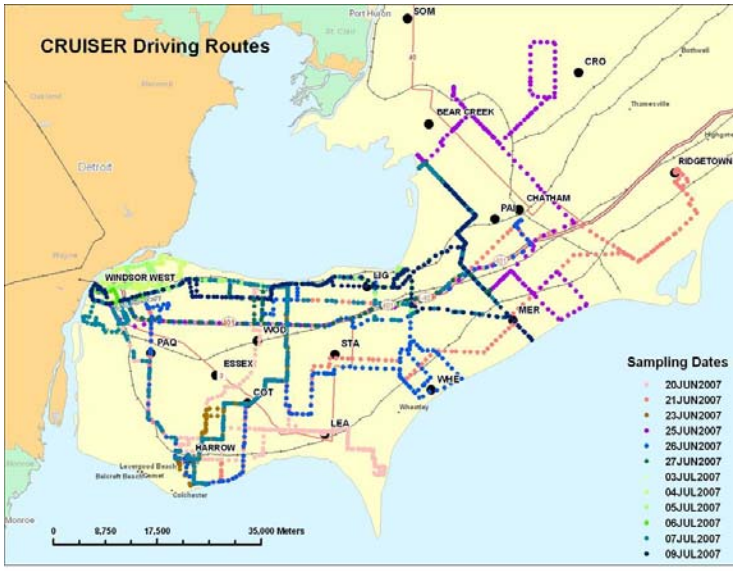

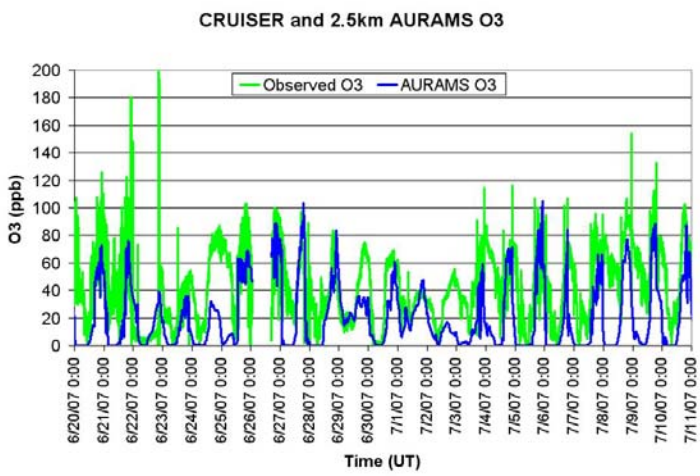

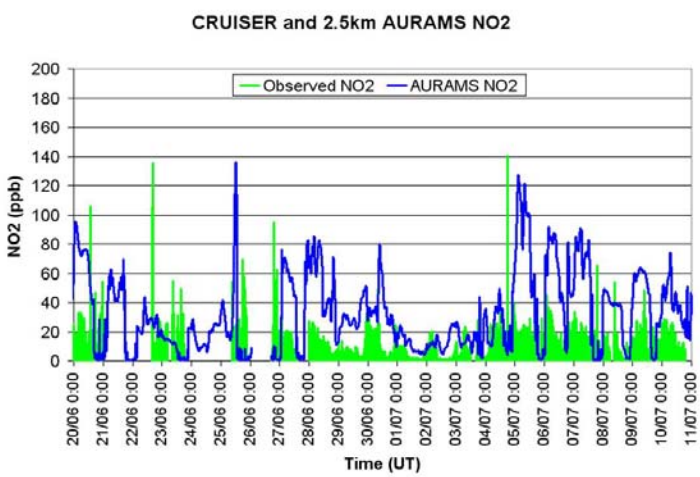

Figure 7: June 26th , 23 UT (7pm local time) (a) Meso-analysis lake-breeze front locations; (b) Lake-breeze front locations inferred from convergence pattern of 2.5-km resolution model winds.

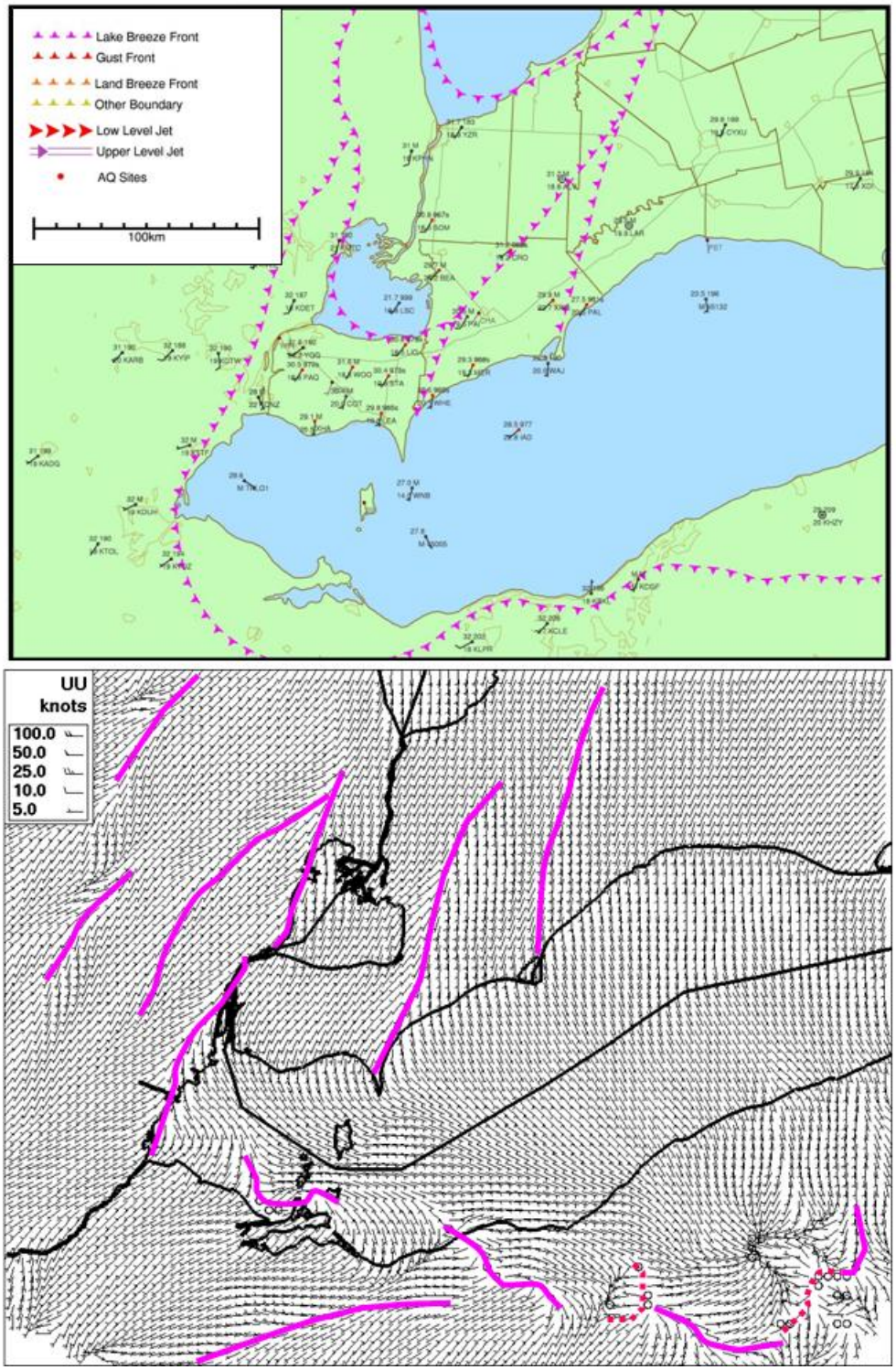

Figure 8: Model-predicted fields for June 26th. 18UT (2pm local time): (a) Surface ozone and wind barbs; (b) Vertical profile of ozone and winds along cross-section A-B. (c,d): As in (a,b), but at 23UT (7 pm local time).

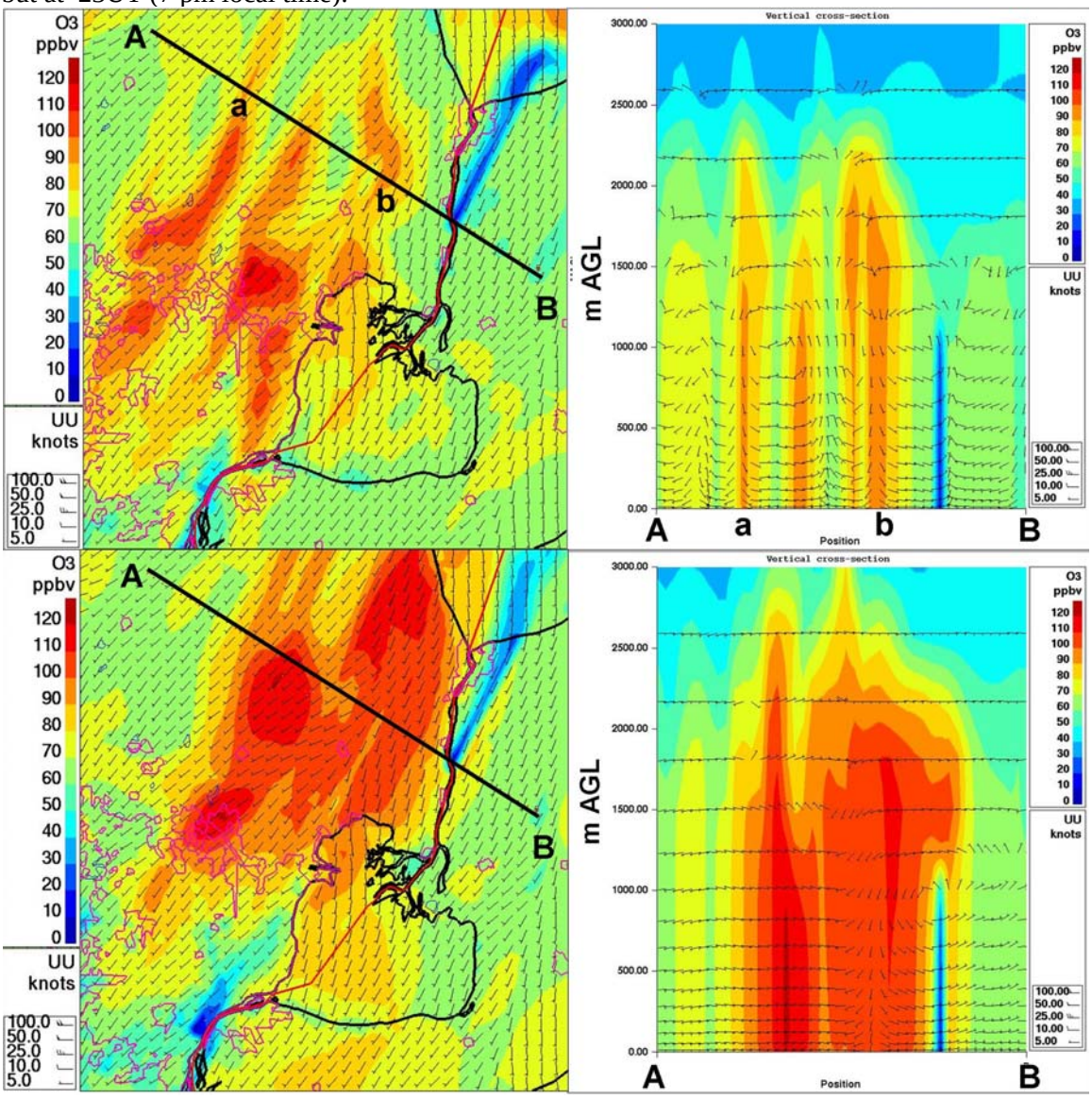

Figure 9: 18UT (2pm local time): (a) Gas-phase photochemical production and loss along cross-section A-B of Fig. 8; (b) Total transport rate of change of ozone along cross-section A-B of Fig 8. (c,d): As in (a,b), but at 23UT (7 pm local time).

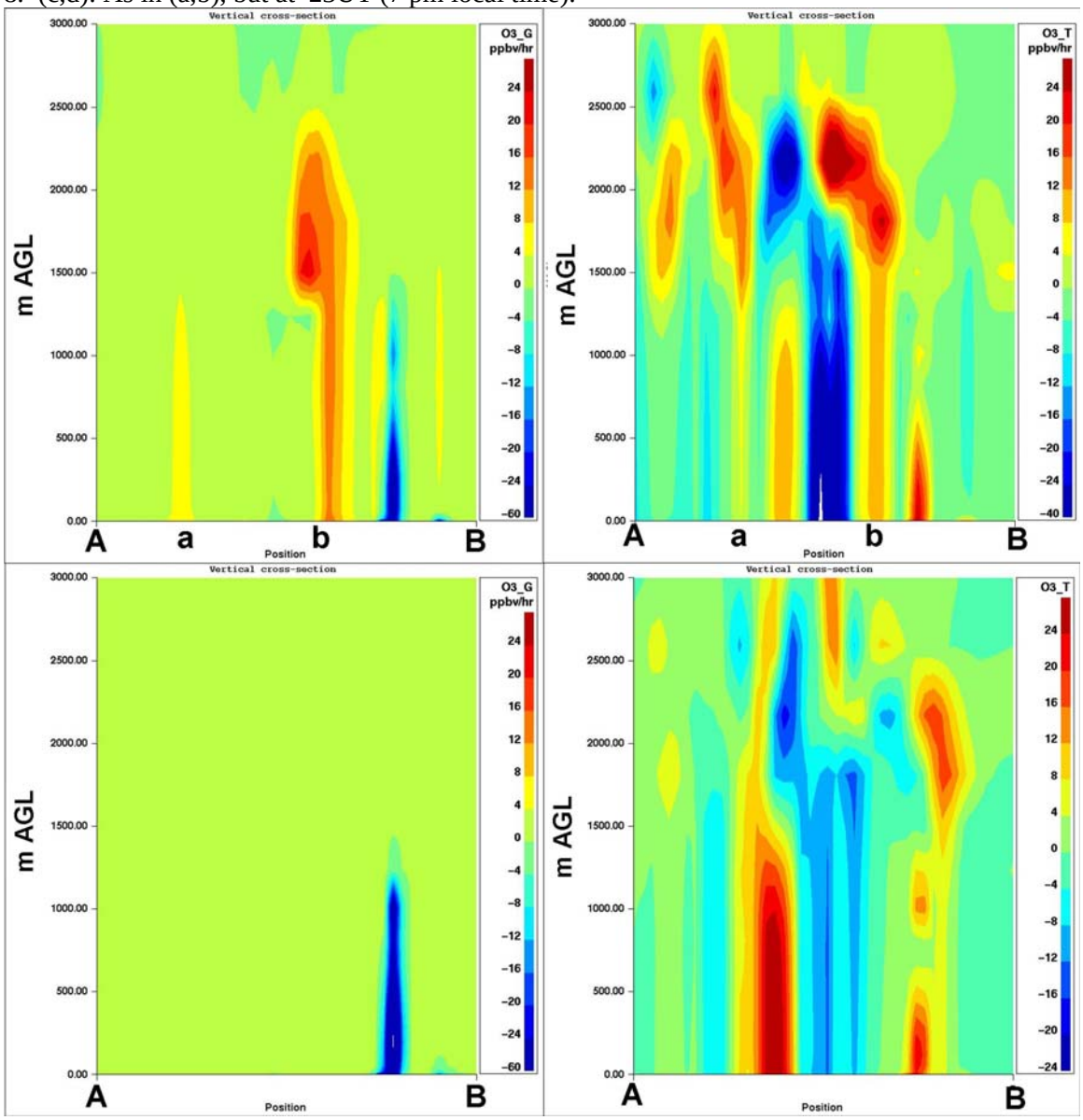

Figure 10: Ozone comparison with surface observations, June 26th, at (a) Paquette Corners, (b) Bear Creek, (c) Grand Bend. Model surface ozone concentrations at (d) 18UT and (e) 23 UT.

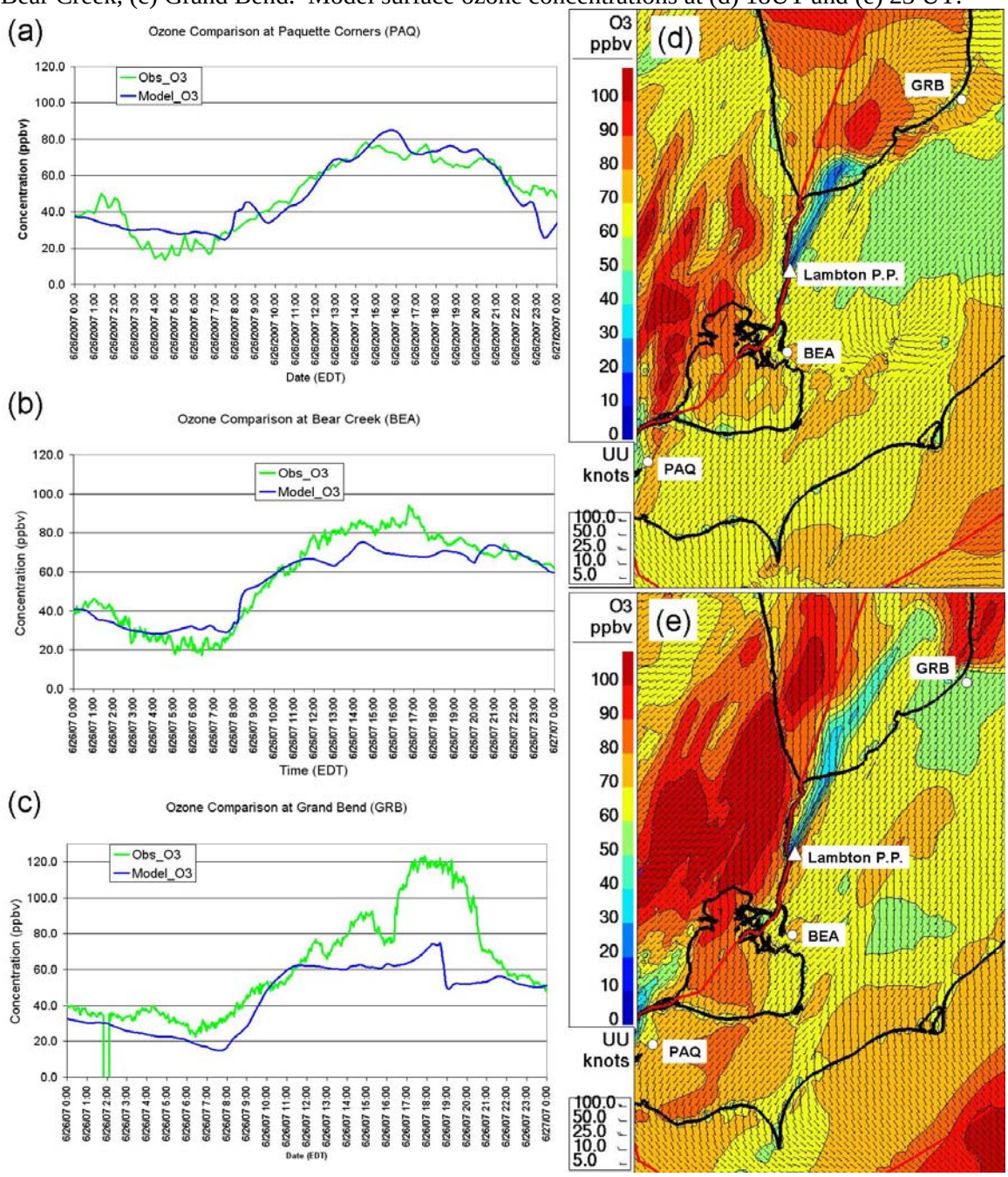

Figure 11: (a) Meso-analysis lake-breeze front locations on July 8th, 17UT (1pm local time); (b) Model-predicted surface wind field and convergence zones.

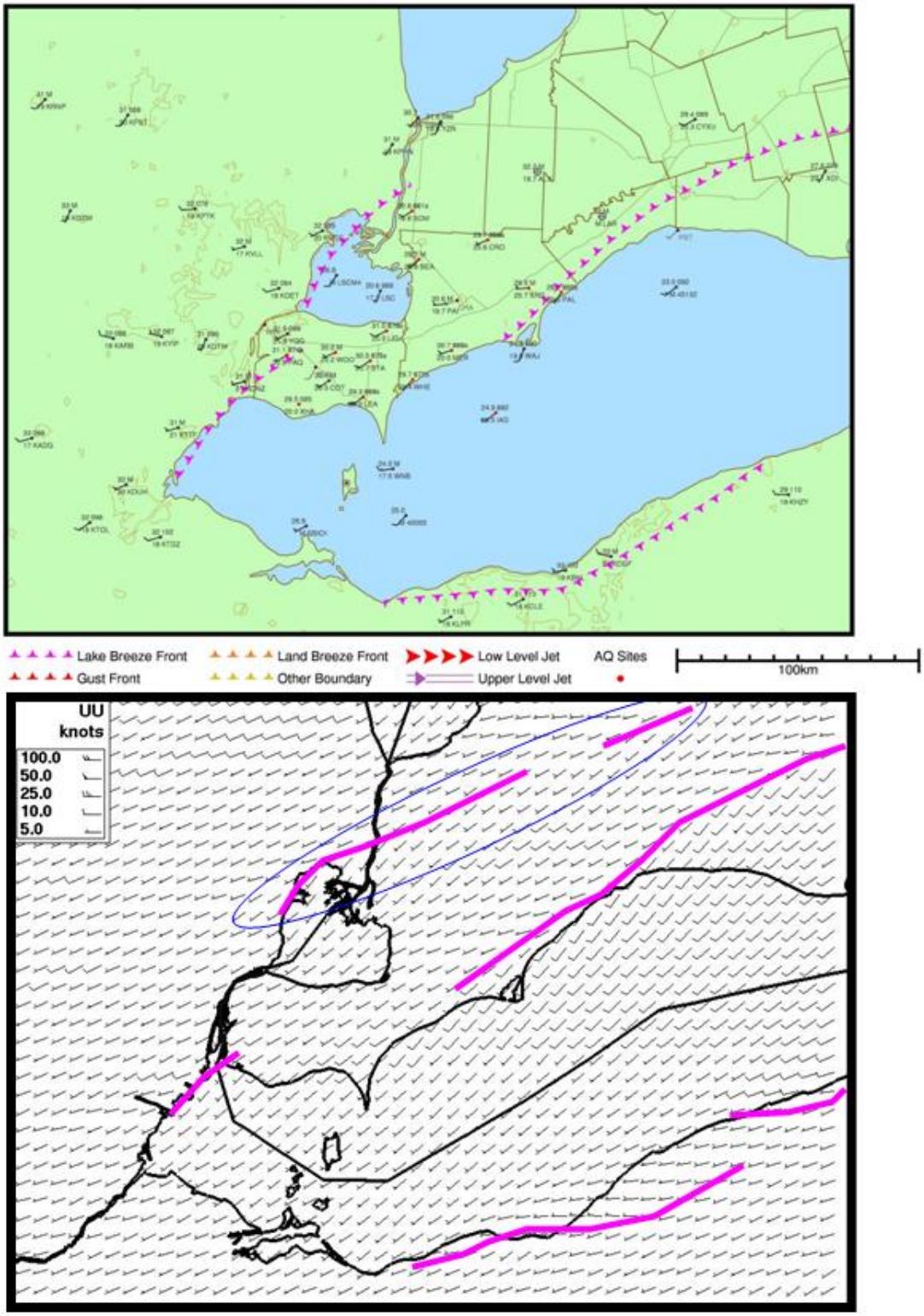

Figure 12: (a) Model-predicted ozone versus observations, July 8th, Sombra station. (b) Model-predicted surface ozone and surface winds at 17 UT (1 pm local time)

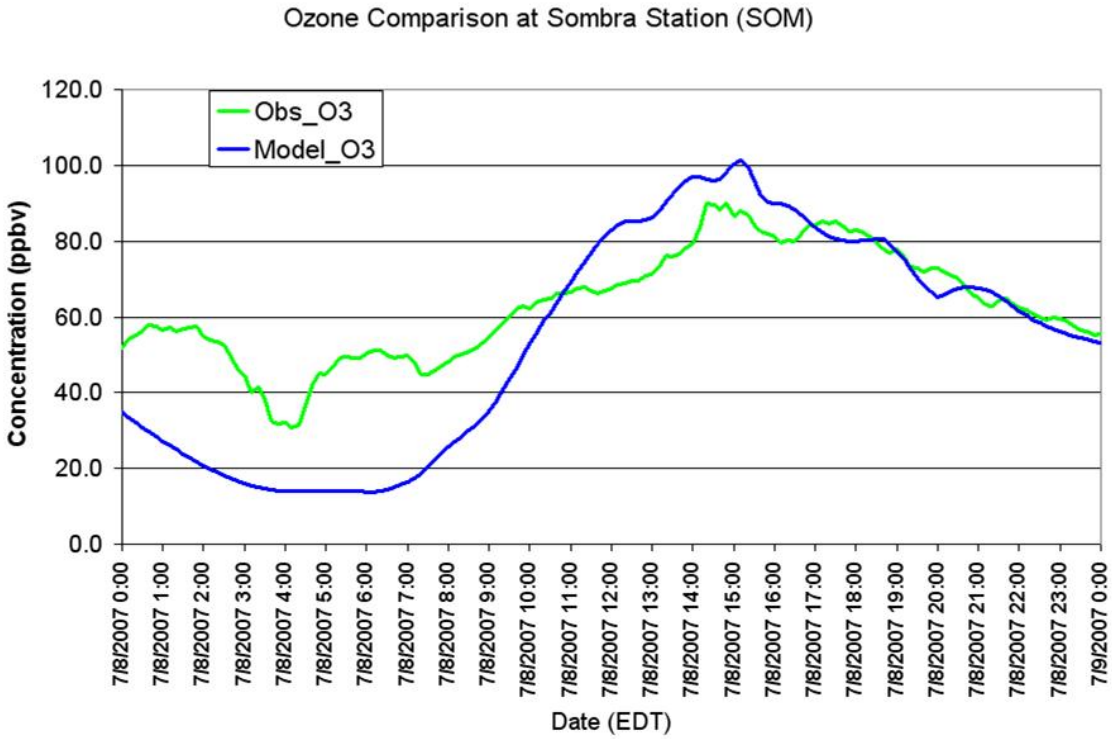

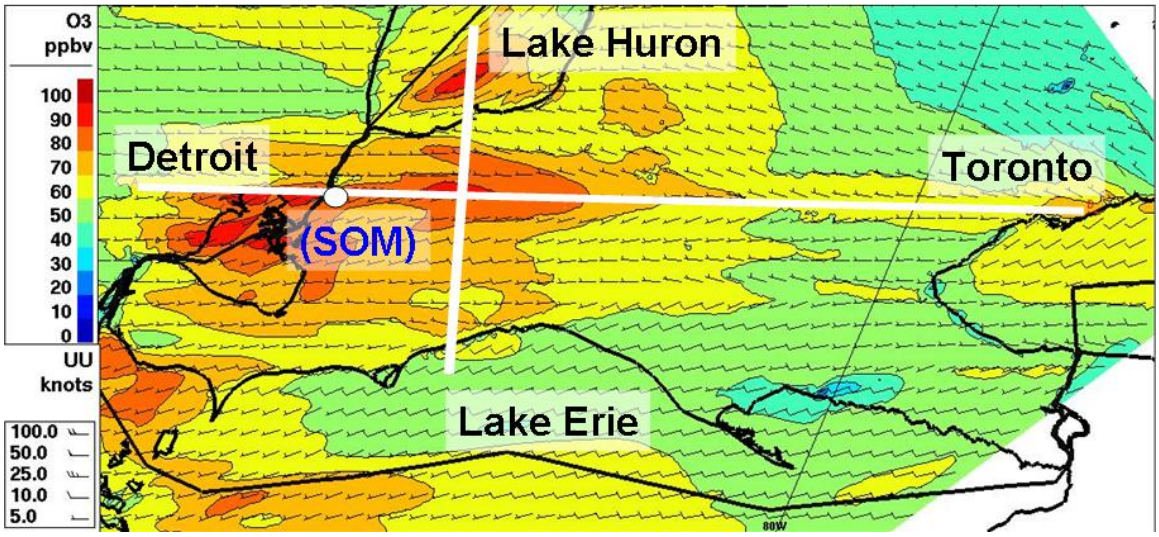

Figure 13: Model-predicted ozone mass tracking fields for July 8th, 17UT (1 pm local time), Detroit to Toronto cross-section. (a) Gas-phase photochemical production, and loss; (b) Total Total transport rate of change.

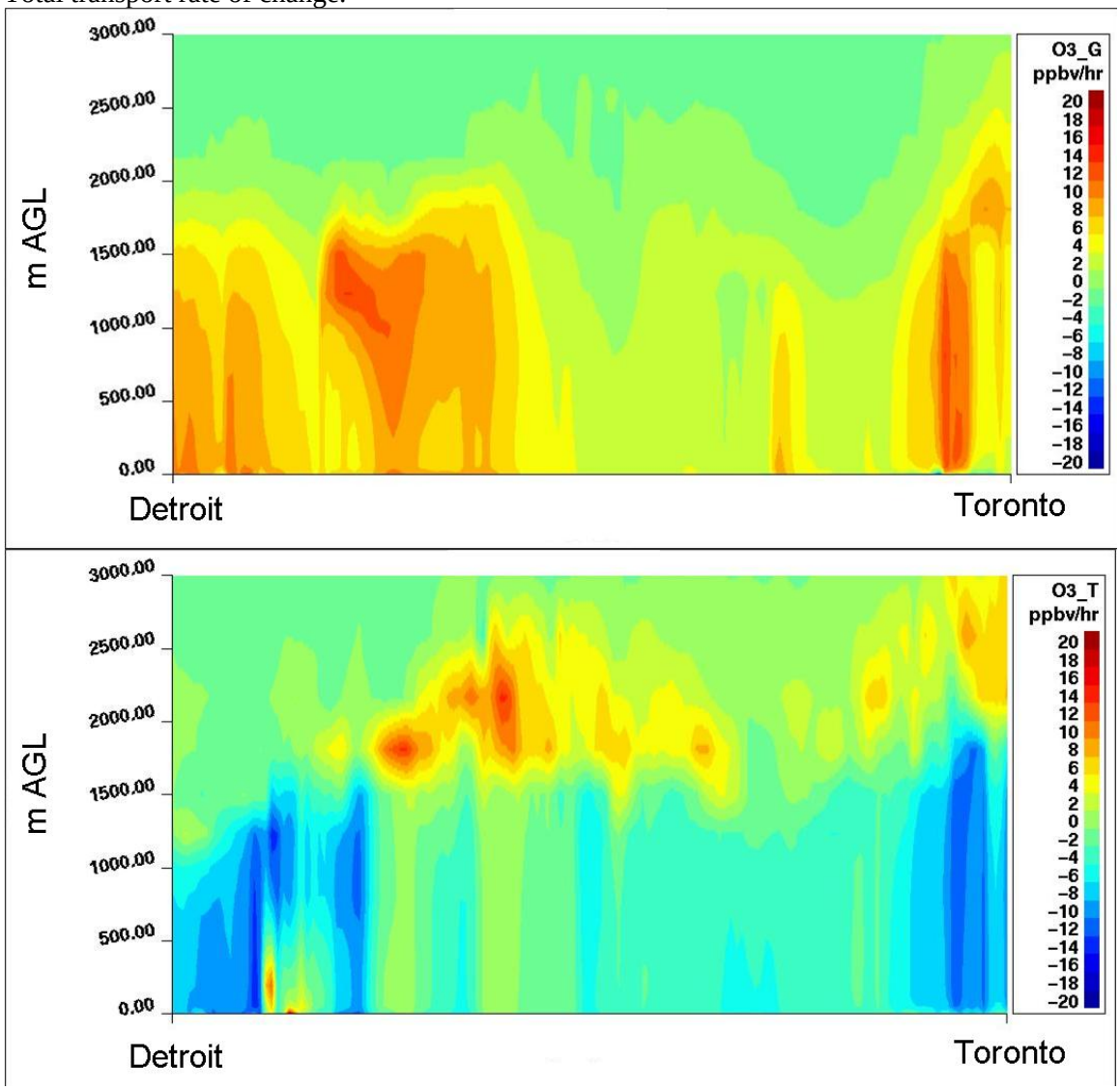

Figure 14: Model-predicted ozone and wind fields, July 8, 17 UT, Lake Huron to Lake Erie cross-section.

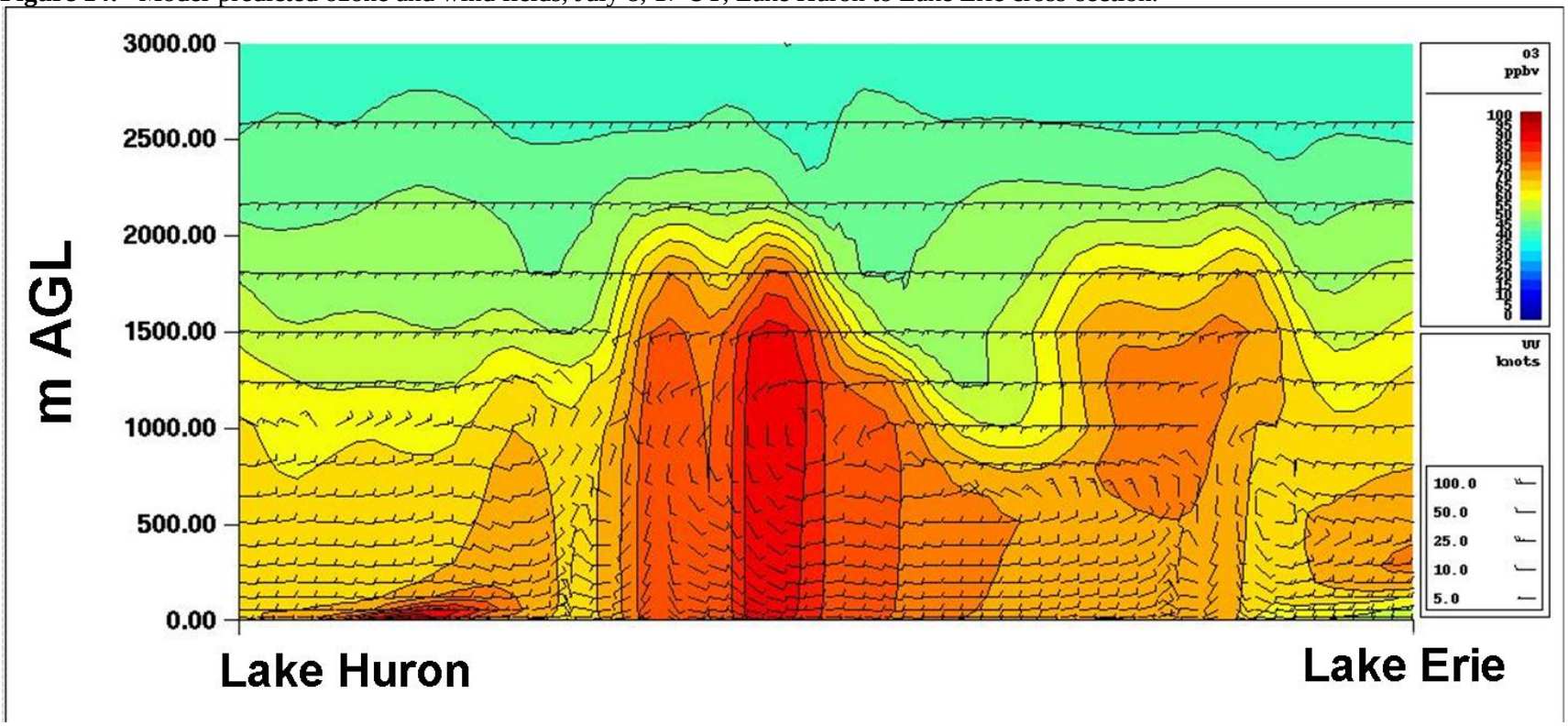

Figure 15: Model-predicted surface ozone and wind fields for July 9th at (a) Croton, (b) Bear Creek. Statistical measures are for the entire measurement intensive, at each site.

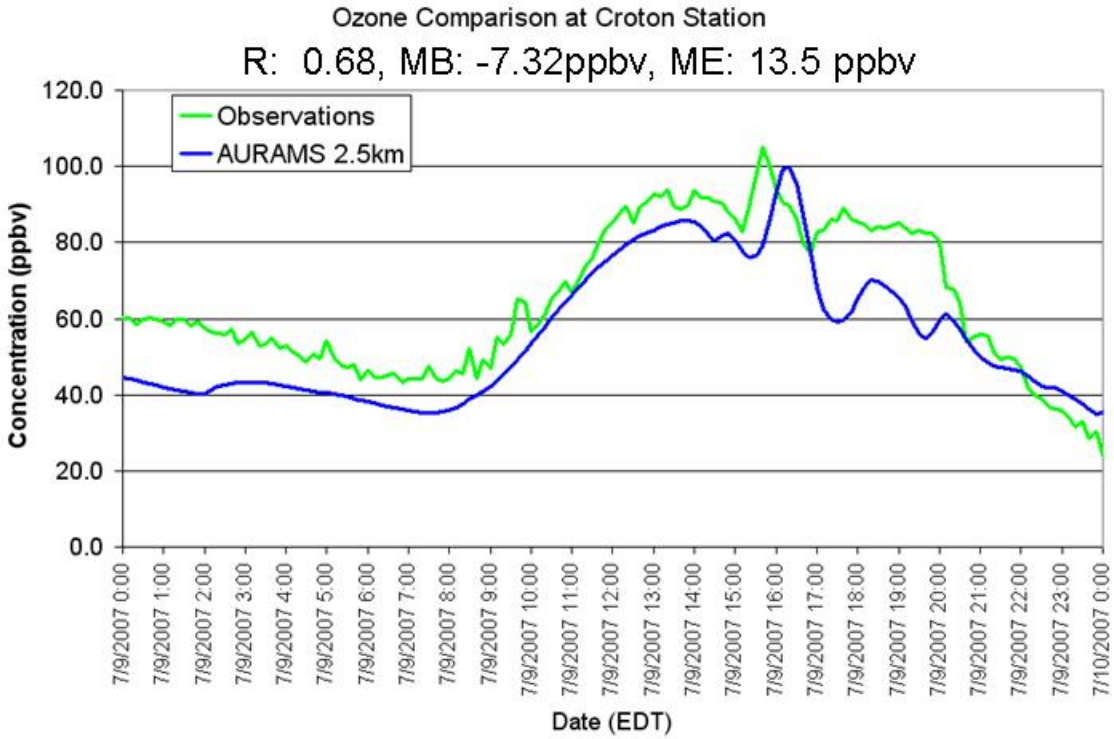

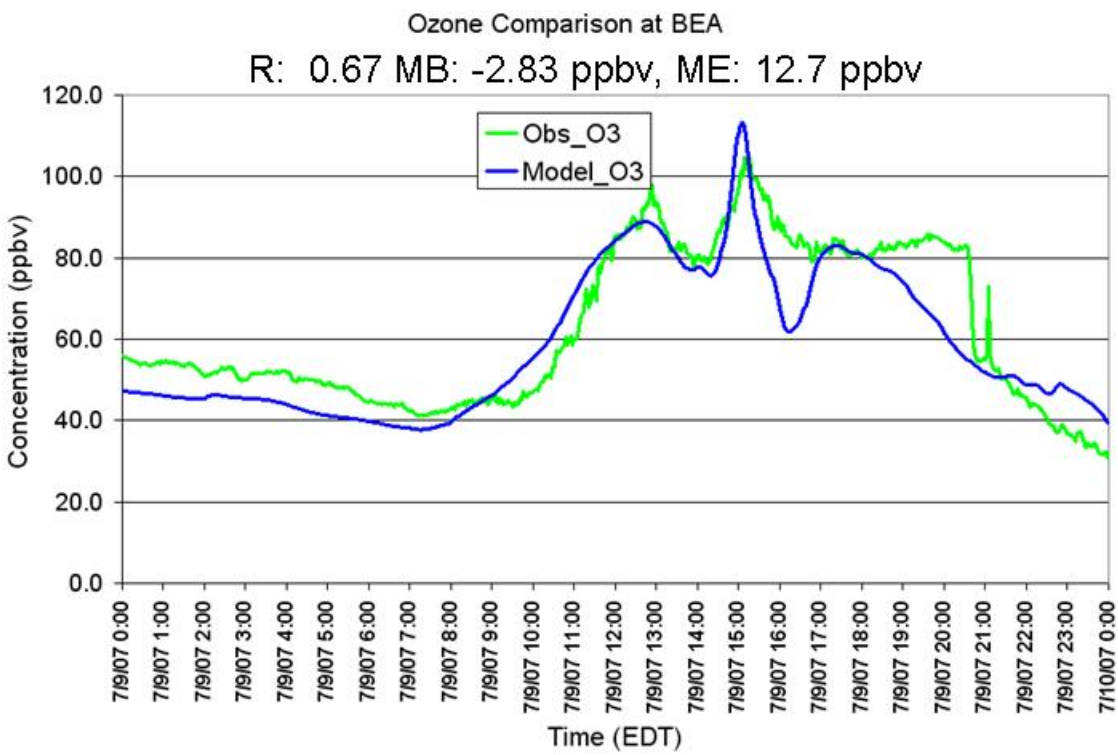

Figure 16: Model-predicted surface ozone and wind fields for July 9th, (a) 17UT (1 pm local time); (b) 19 UT (3 pm); (c) 20 UT (4pm); (d) 22 UT (6pm). SOM: Sombra station. CRO: Croton station. Lambton P.P. = Lambton Power-Plant

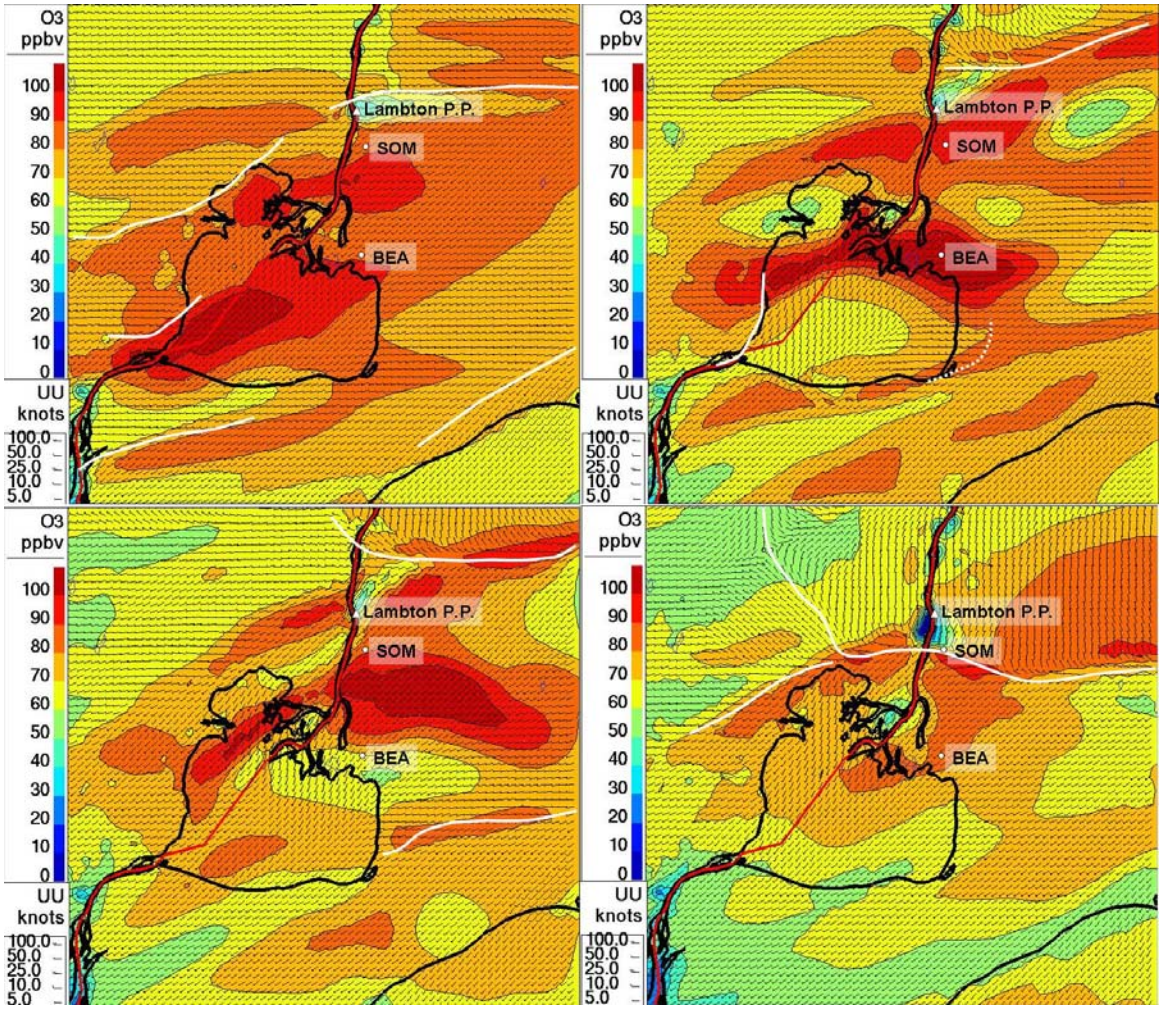

Figure 17: 23 day average wind fields at (a) 12UT, (b) 16 UT, (c) 20 UT, and (d) 0 UT; 8 am, 12 pm, 4 pm and 8 pm, respectively. Convergence regions marked as solid mauve lines, boundary of divergence outflow regions marked with dashed mauve lines.

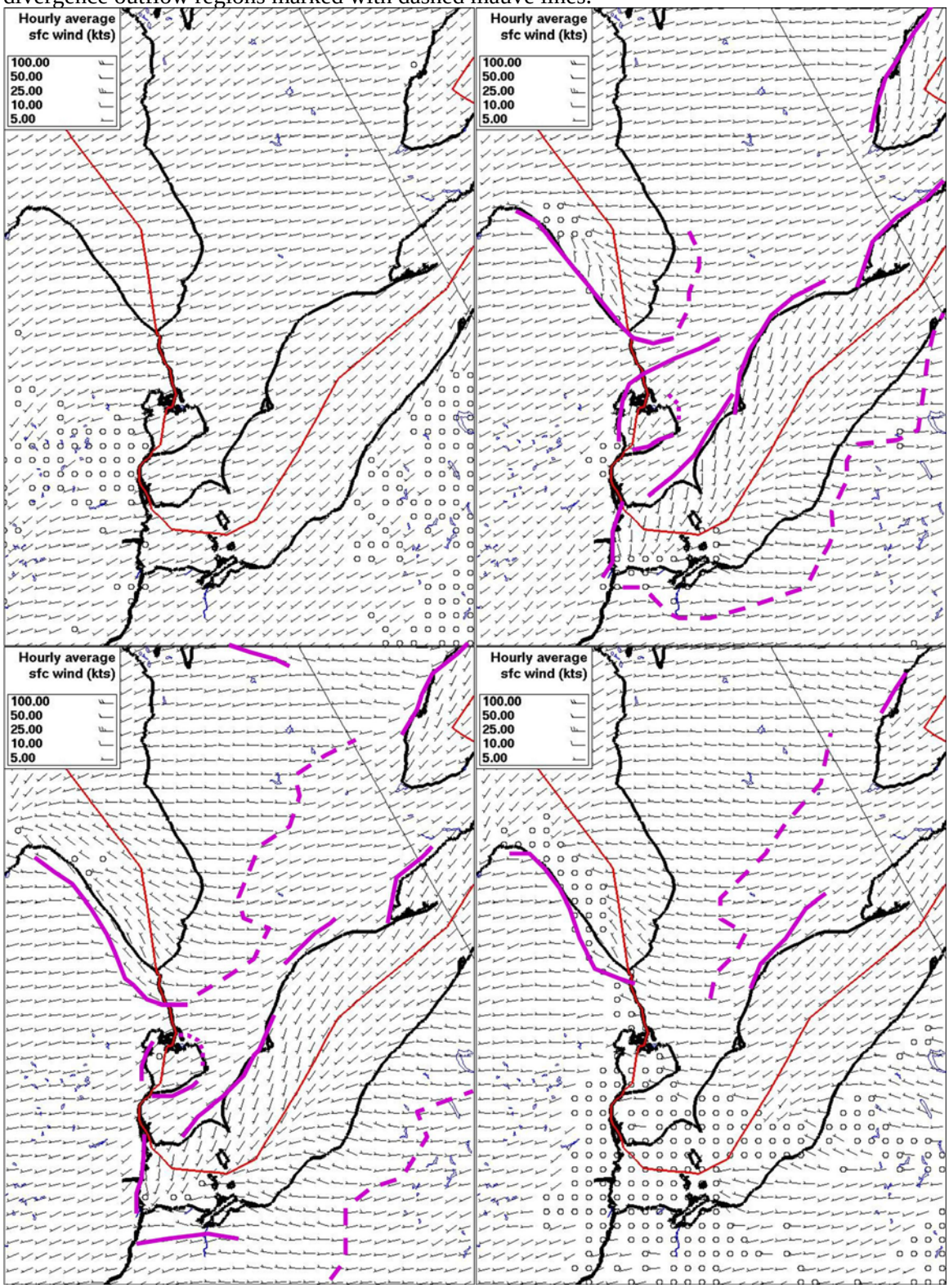

Figure 18: 23 day average ozone concentration fields at (a) 12UT, (b) 16 UT, (c) 20 UT, and (d) 0 UT; 8 am, 12 pm, 4 pm and 8 pm, respectively.

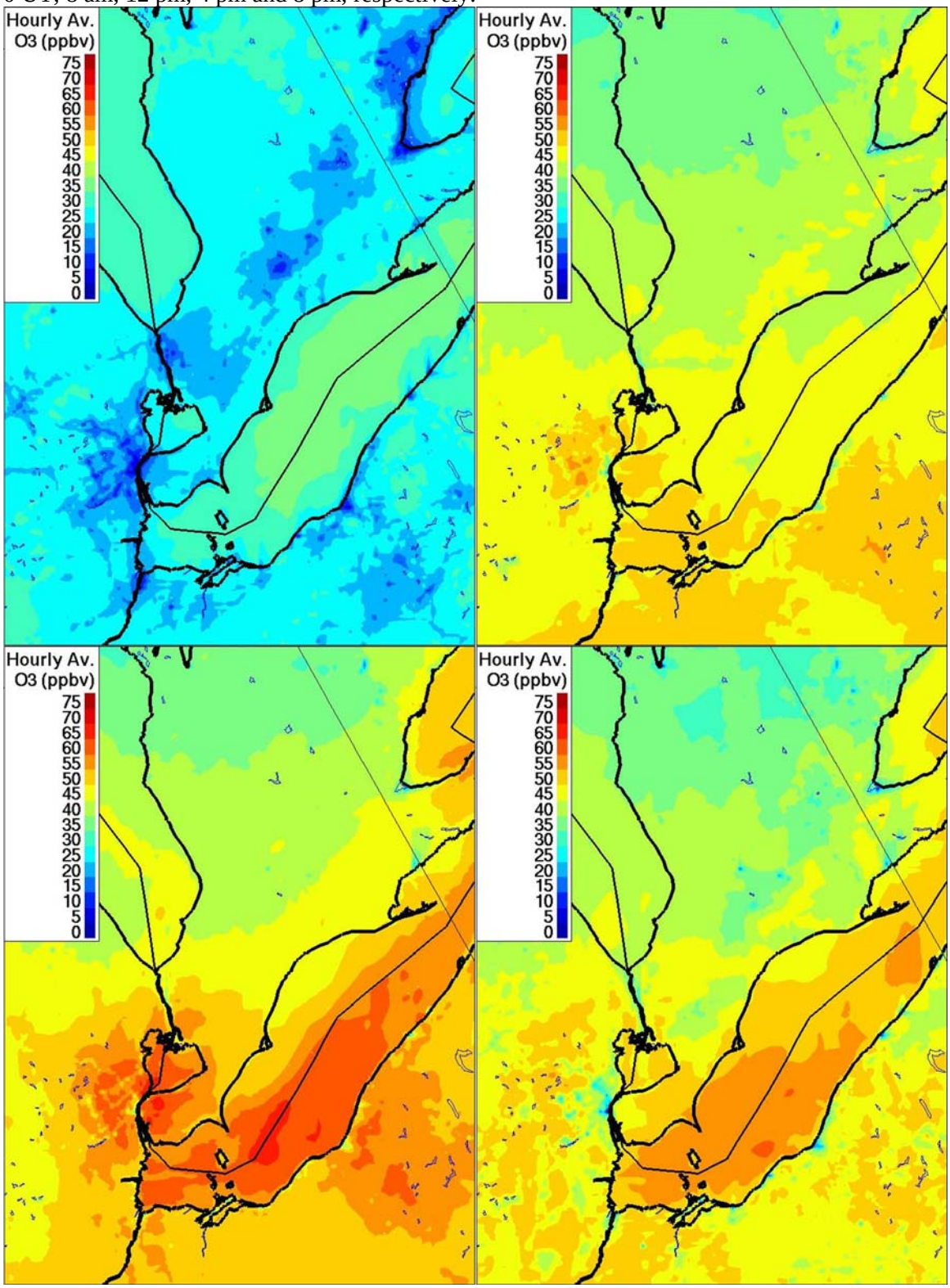

Figure 19: 23 day average values at 20Z (4 pm local time): (a) Surface ozone over Lake St. Clair and Lake Erie, showing location of cross-section used for (b) ozone concentration, (c) ozone gas-phase production and loss, (d) ozone total transport.

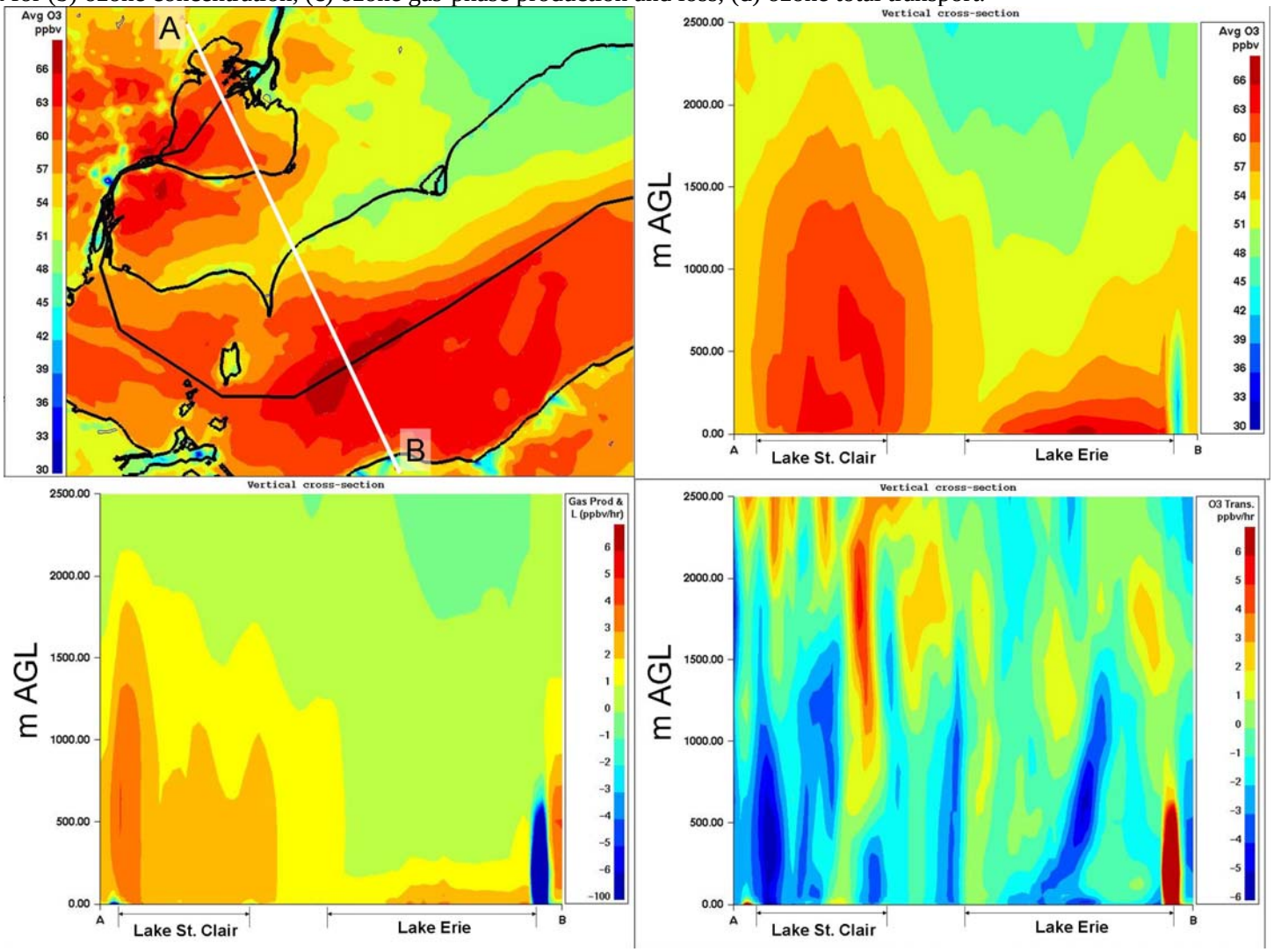
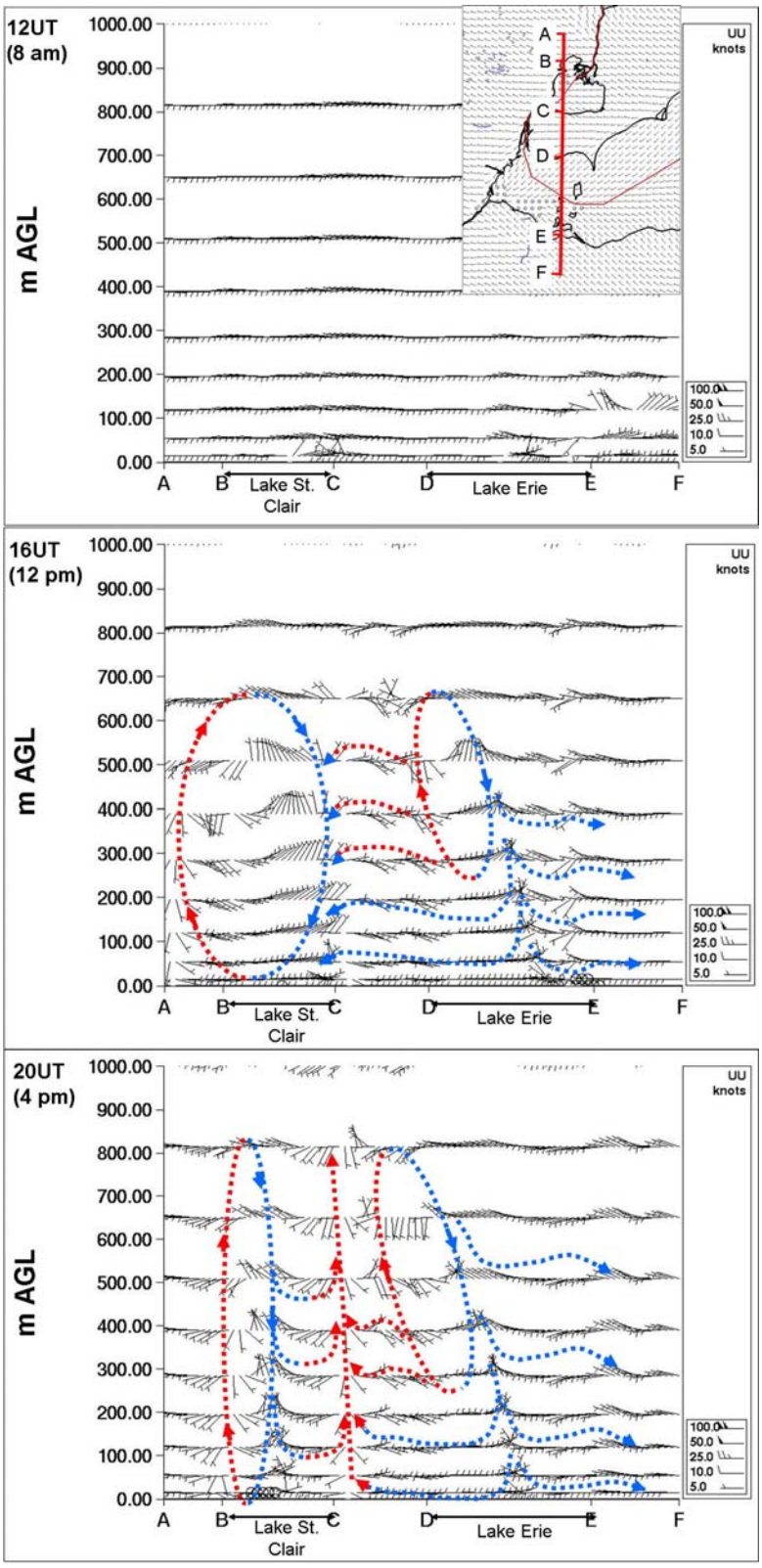
Figure 20: Cross-section of 3D wind fields across Lakes St. Clair and Erie at (a) 12UT (8am), (b)_ 16UT (12 noon), and (c) 20 UT (4pm). Net upward motion streamlines are sketched in red, downward motion in blue. Inset: location of the cross-section, superimposed on 20UT surface winds.